A Keck/DEIMOS spectroscopic survey of faint Galactic satellites: searching for the least massive dwarf galaxies[*]

N. F. Martin,[1]† R. A. Ibata,[2] S. C. Chapman,[3,4]‡ M. Irwin[3] and G. F. Lewis[5]

[1]*Max-Planck-Institut für Astronomie, Königstuhl 17, D-69117 Heidelberg, Germany*
[2]*Observatoire de Strasbourg, 11, rue de l'Université, F-67000 Strasbourg, France*
[3]*Institute of Astronomy, Madingley Road, Cambridge CB3 0HA*
[4]*Department of Physics and Astronomy, University of Victoria, Victoria, BC, Canada V8P 1A1*
[5]*Institute of Astronomy, School of Physics, A29 University of Sydney, NSW 2006, Australia*

ABSTRACT

We present the results of a spectroscopic survey of the recently discovered faint Milky Way satellites Boötes, Ursa Major I, Ursa Major II and Willman 1 (Wil1). Using the DEep Imaging Multi-Object Spectrograph mounted on the Keck II telescope, we have obtained samples that contain from $\sim$15 to $\sim$85 probable members of these satellites for which we derive radial velocities precise to a few km s^{-1} down to $i \sim 21$–22. About half of these stars are observed with a high enough signal-to-noise ratio to estimate their metallicity to within $\pm$0.2 dex. The characteristics of all the observed stars are made available, along with those of the Canes Venatici I dwarf galaxy that have been analysed in a companion paper.

From this data set, we show that Ursa Major II is the only object that does not show a clear radial velocity peak. However, the measured systemic radial velocity ($v_r = 115 \pm 5 \,\mathrm{km\,s^{-1}}$) is in good agreement with simulations in which this object is the progenitor of the recently discovered Orphan Stream. The three other satellites show velocity dispersions that make them highly dark matter dominated systems (under the usual assumptions of symmetry and virial equilibrium). In particular, we show that despite its small size and faintness, the Wil1 object is not a globular cluster given its metallicity scatter over $-2.0 \lesssim \mathrm{[Fe/H]} \lesssim -1.0$ and is therefore almost certainly a dwarf galaxy or dwarf galaxy remnant. We measure a radial velocity dispersion of only $4.3^{+2.3}_{-1.3}\,\mathrm{km\,s^{-1}}$ around a systemic velocity of $-12.3 \pm 2.3\,\mathrm{km\,s^{-1}}$ which implies a mass-to-light ratio of $\sim$700 and a total mass of $\sim 5 \times 10^5\,\mathrm{M_\odot}$ for this satellite, making it the least massive satellite galaxy known to date. Such a low mass could mean that the $10^7\,\mathrm{M_\odot}$ limit that had until now never been crossed for Milky Way and Andromeda satellite galaxies may only be an observational limit and that fainter, less massive systems exist within the Local Group. However, more modelling and an extended search for potential extratidal stars are required to rule out the possibility that these systems have not been significantly heated by tidal interaction.

Key words: galaxies: dwarf – galaxies: kinematics and dynamics – Local Group – dark matter.

1 INTRODUCTION

The discrepancy between observed satellite galaxies in the Local Group and the number of dark matter haloes that are produced in simulations of such groups of galaxies is a well-known problem of the currently preferred Lambda cold dark matter (ΛCDM) cosmology (Klypin et al. 1999; Moore et al. 1999). Various explanations have been put forward to explain this difference of one to two orders of magnitudes between the observed and simulated number

of satellites, with most of them assuming that the satellite dwarf galaxies observed within the Local Group are surrounded by massive dark matter haloes and that they become even more highly dark matter dominated as they become fainter (e.g. Bullock, Kravstov & Weinberg 2000; Stoehr et al. 2002). In this way, even faint satellites would reside in massive dark matter haloes and would only represent the more massive end of the distribution of dark haloes found in simulations, hence reconciling observations and simulations.

The central velocity dispersion of spherical systems in virial equilibrium can be used to derive the total mass of the system (e.g. Illingworth 1976; Richstone & Tremaine 1986). Even though dwarf galaxies orbiting within the Local Group may not be in virial equilibrium or perfectly spherical systems, the central velocity dispersion has been shown to be a good indicator of the instantaneous mass of the galaxy (e.g. Oh, Lin & Aarseth 1995; Piatek & Pryor 1995). Hence spectroscopic observations of faint dwarf galaxies discovered these past few years within wide-field surveys, in particular with the Sloan Digital Sky Survey (SDSS), have been rapidly conducted. They seem to show a mass limit of $\sim 10^7\,\mathrm{M}_\odot$ under which no dwarf galaxy can be found, meaning these satellites would indeed inhabit massive dark matter haloes. In particular, one can cite masses of $\sim 10^7$ for Ursa Major I (Kleyna et al. 2005), $\sim 2 \times 10^7$ for Andromeda IX (Chapman et al. 2005) and $\sim 1 \times 10^7$ for Boötes (Muñoz et al. 2006) in solar units. The existence of such a mass limit would confirm the empirical relation defined by Mateo (1998) for satellites that are brighter than Draco ($M_V = -8.8$) and Ursa Minor ($M_V = -8.9$) in the Local Group: $M/L = 2.5 + 10^7/(L/\mathrm{L}_\odot)$ where M/L is the mass-to-light ratio of the galaxies and L their luminosity. Some groups have been working on the theoretical aspects of the existence of such a limit, in order to explain it in the ΛCDM context. In particular, the recent work of Read, Pontzen & Viel (2006) explains this limit by the effect of supernova winds that produce a sharp drop of around two orders of magnitude of the stellar mass over the total (stellar and dark matter) mass range $3\text{--}10 \times 10^7\,\mathrm{M}_\odot$. They conclude their work by predicting that galaxies a few orders of magnitude fainter than Draco, Ursa Minor or even Ursa Major I ($M_V \sim -6.75$; Willman et al. 2005b) should still have total masses within the $2\text{--}10 \times 10^7\,\mathrm{M}_\odot$ range.

However, the measured mass distribution of faint dwarf galaxies within the Local Group has until now been mainly limited by the low number of such objects for which a radial velocity survey has been conducted. With the recent discovery of ~ 15 new satellites around the Milky Way (Willman et al. 2005a,b; Belokurov et al. 2006a,b; Zucker et al. 2006a,b) and the Andromeda galaxy (Zucker et al. 2004; Chapman et al. 2005; Martin et al. 2006; Zucker et al. 2007), all of them with $M_V \gtrsim -8.0$, it is now possible to populate the faint end of the satellite mass distribution and see if the $10^7\,\mathrm{M}_\odot$ mass limit still holds for such faint systems and if they are indeed highly dark matter dominated. As a first step towards this end, we have used the DEep Imaging Multi-Object Spectrograph (DEIMOS) on Keck II to derive radial velocities and metallicities for stars within the Boötes (Boo), Canes Venatici I (CVnI), Ursa Major I (UMaI), Ursa Major II (UMaII) and Willman 1 (Wil1) Milky Way satellites. The analysis of our observations is performed here for all these objects, except for CVnI which has been analysed in a companion paper (Ibata et al. 2006), where we presented in more detail its peculiar kinematic behaviour. The outline of the paper is as follows: Section 2 presents the observing strategy, the observations and how they were reduced; Sections 3–7 are dedicated to the analysis of Boo, CVnI, UMaI, UMaII and Wil1 and we conclude in Section 8.

2 OBSERVATIONS

Target stars were selected for observation from the point sources in the fourth data release (DR4) of the SDSS (see Fig. 1). Stars of highest priority were chosen within a polygon defined by eye around the probable red giant branches (RGBs) of the target satellites (see Fig. 2), while all other available point sources within the fields were assigned a lower priority. The DEIMOS configuration programme was then used to automatically design the masks.

For Boo, CVnI and UMaI, two DEIMOS masks were observed, slightly offset in declination, whereas only one field in each of UMaII and Wil1 were observed. A planned northern mask in UMaII was not observed due to time constraints, which accounts for the offset in Fig. 1. Each mask was observed with three exposures of 1200 s with the 1200 lines mm^{-1} grating during the nights of 2006 May 27 and 28. These settings give access to the 650–900 nm spectral region and along with slits of 0.7 arcsec width result in 1-Å resolution spectra. Contrary to the normal operations with DEIMOS, we observed an arc-lamp spectrum immediately before and after each set of science frames, in order to ensure a better wavelength calibration than is possible from day-time arc-lamp exposures.

The science spectra were extracted and processed in an identical manner to that described in Ibata et al. (2006). In particular, the final stage comprised a Gaussian fit to each of the Ca II triplet lines independently, which also yields a robust velocity uncertainty from the rms scatter of the three resulting velocities. All targets discussed below have signal-to-noise ratio (S/N) > 2.0 Å^{-1} and $v_{err} < 15\,\mathrm{km\,s^{-1}}$. We also measure the [Fe/H] metallicities from the equivalent widths (EWs) of the Ca II lines (Rutledge, Hesser & Stetson 1997). The metallicities are placed on the Carretta & Gratton (1997) scale using the relation [Fe/H] $= -2.66 + 0.42[\Sigma\mathrm{Ca} + 0.64(V - V_{HB})]$ where $\Sigma\mathrm{Ca} = 0.5\mathrm{EW}_{\lambda 8498} + 1.0\mathrm{EW}_{\lambda 8542} + 0.6\mathrm{EW}_{\lambda 8662}$ and $(V - V_{HB})$ is a surface gravity correction relative to the V-band magnitude of the star, V, and the V-band magnitude of the horizontal branch of the satellite it is assumed to belong to, V_{HB}.[1] V-band fluxes are calculated from the SDSS colours using transformations derived by our group (Ibata et al. 2007). V_{HB} is determined from the colour–magnitude diagrams (CMDs) for the satellite that show a horizontal branch (HB) (Boo, CVnI and UMaI, see Fig. 2) and is fixed as $V_{HB} = m - M + 0.7$ for the two others (UMaII and Wil1). Although this is an approximate estimate, [Fe/H] is not very sensitive to this quantity since [Fe/H] $\propto 0.27(V - V_{HB})$. Previous experience has shown that S/N > 15 Å^{-1} spectra have uncertainties of ~ 0.2 dex on their [Fe/H] value with this method, although this does not account for systematic shifts that might come from the assumed metallicity scale.

The spectra are then shifted to the rest frame, and we measure the EW of the Na I doublet lines at 8183.25 and 8194.82 Å by two Gaussian fits (with fixed centroids for the two lines). These lines are gravity sensitive and can be used to discriminate foreground dwarf stars from the targeted giant stars belonging to the Milky Way satellites (Schiavon et al. 1997).

In Fig. 3, the sum of the Na I EWs, $\Sigma\mathrm{Na} = \mathrm{Na}_{\lambda 8193} + \mathrm{Na}_{\lambda 8195}$, is compared for stars selected to belong to the CMD features of the satellites (RGB and HB) and represented as filled circles and field stars chosen in the same magnitude range (hollow circles). It is readily visible that satellite stars have much lower $\Sigma\mathrm{Na}$ values than field stars, as is expected for giant stars with lower surface gravity.

---

[1] The metallicity of each star in the sample is determined assuming the distance of the satellite it might belong to. Thus, the derived values are not meaningful if the star is not a satellite member.
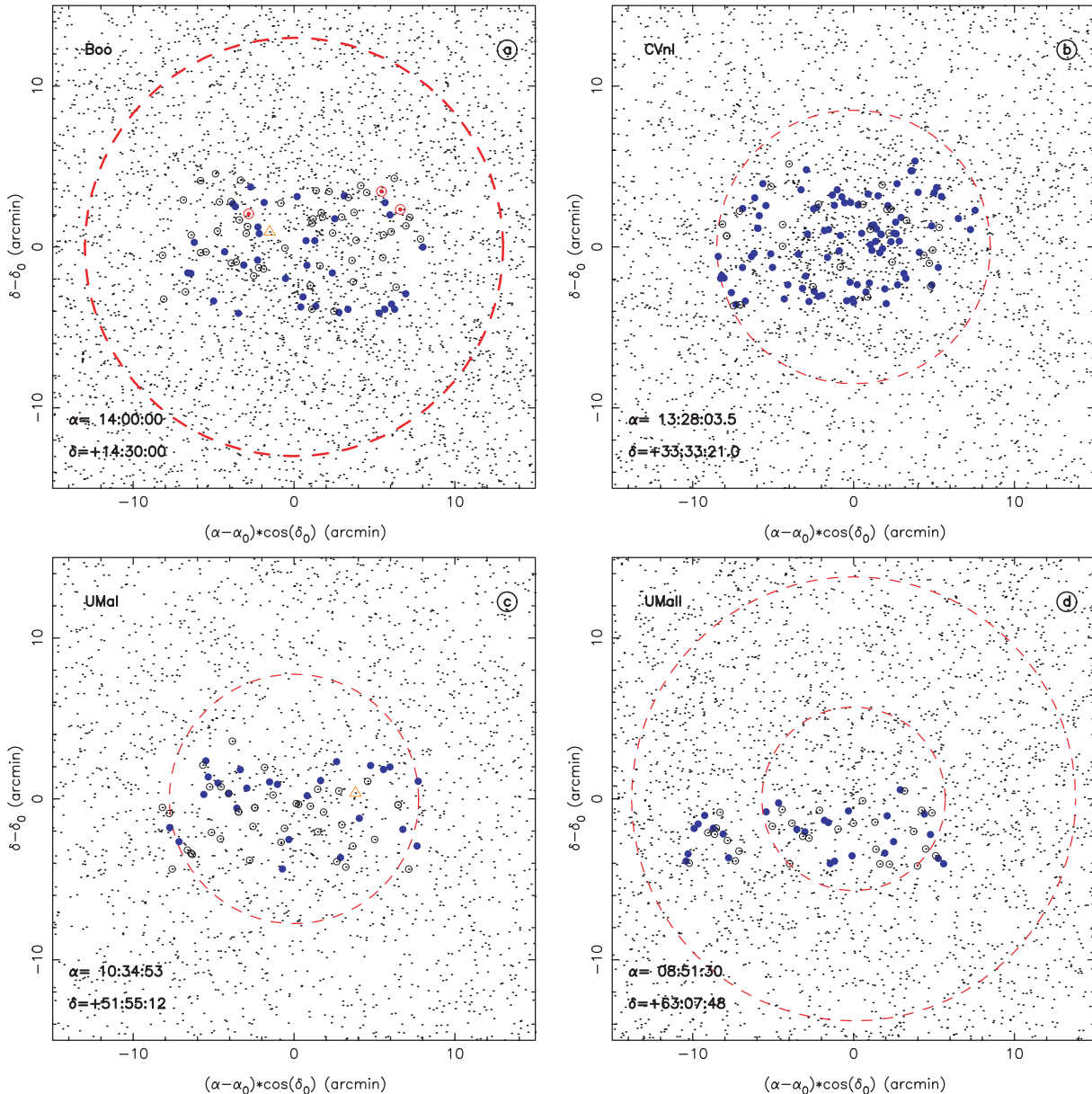
Figure 1. The SDSS point sources around the five Milky Way satellites observed in our survey (a: Boo, b: CVnI, c: UMaI, d: UMaII and e: Wil1). Small dots represent all the SDSS stars in the region, filled circles represent target stars selected from the CMD of the satellites (RGB and main-sequence turn-off stars that have a low Na doublet EW; see Figs 2 and 3). Hollow circles represent field stars that were selected in the same magnitude range or stars that do not pass the Na doublet threshold and are likely foreground dwarf stars. They are not related to the satellite. In panel (a), circled big points represent stars that were initially selected as field stars but have the radial velocity and the CMD position of Boo stars; they are included in the analysis to derive Boo parameters. In panels (a) and (c), triangles represent stars selected along the RGB of the satellites but that have [Fe/H] > −1.0 and are probably not related to the metal-poor satellites. The dashed lines in all panels correspond to the half-light radius (in the case of UMaII, panel (d), the two limits of the half-radius measured by Zucker et al. 2006b are shown). *[This Figure is available in colour in the online version of the journal.]*

This effect is most visible for the populous samples of Boo and CVnI. From these, we will use $\Sigma Na = 0.8$ as the threshold between giant stars belonging to the Milky Way satellites and foreground contaminating dwarf stars. It remains a perfectly valid threshold for UMaI and Wil1 though in both cases there is one star that was selected along the RGB of the satellite and with a slightly higher ΣNa that is hence not considered as a satellite star. Since in these two cases, the satellite and Galactic contamination radial velocities overlap, we prefer removing a potential satellite star in order to have a more secure sample. In the case of UMaII ΣNa does not seem to

be as efficient in separating dwarf from giant stars although the data are of similar quality (see Section 6 for more details).

3 BOÖTES

Boo was discovered in the SDSS as an overdensity of stars that are aligned in the CMD and follow a well-defined red giant and HB (Belokurov et al. 2006a). Although very faint ($M_V = −5.8 \pm 0.5$, but this value may be underestimated, see Muñoz et al. 2006), this new Milky Way satellite has characteristics typical of dwarf
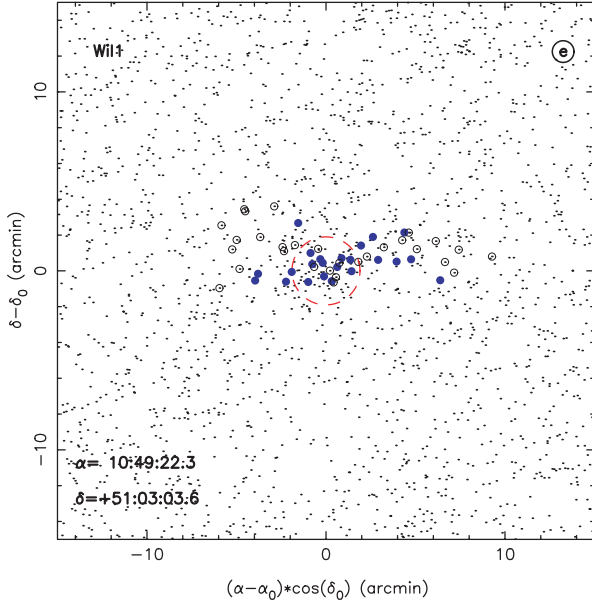
Figure 1 – *continued*

galaxies with a half-light radius of 227 ± 13 pc (Belokurov et al. 2006a), a heliocentric distance of 62 ± 3 kpc (determined from RR Lyrae stars; Siegel 2006) and is dominated by a metal-poor population with estimates ranging from [Fe/H] ∼ −2.5 (Muñoz et al. 2006; Siegel 2006) to [Fe/H] = −2.0 (Siegel 2006). A first spectroscopic analysis of the dwarf galaxy has been performed by Muñoz et al. (2006) and among their 58 targets, the seven Boo members that are within the half-light radius yield a systemic velocity and velocity dispersion of $v_r = 95.6 \pm 3.4\,\mathrm{km\,s^{-1}}$ and $\sigma_{v_r} = 6.6 \pm 2.3\,\mathrm{km\,s^{-1}}$, respectively. As is often done for such studies, they use this velocity dispersion to derive a total mass of $\sim 1 \times 10^7\,\mathrm{M_\odot}$ for the system, implying an M/L that is higher than 100 in solar units.

Fig. 4 summarizes the spectroscopic information of our Boo sample observed with DEIMOS and Table 1 lists the individual data on each observed star. In the central panel of the figure, there is a clear separation between foreground dwarf stars with ΣNa > 0.8 (hollow circles) and stars that are aligned along the CMD features of the dwarf galaxy (filled circles) which are clustered around ∼100 km s⁻¹ as expected. However, three of the field stars fall within the Boo peak. Since they are also close to the RGB and HB of the dwarf galaxy and have ΣNa < 0.8, we consider them as Boo members (the circled big dots of Figs 2a, 3a and 4). One of the stars in the sample, represented by a triangle in Fig. 4, has a radial velocity

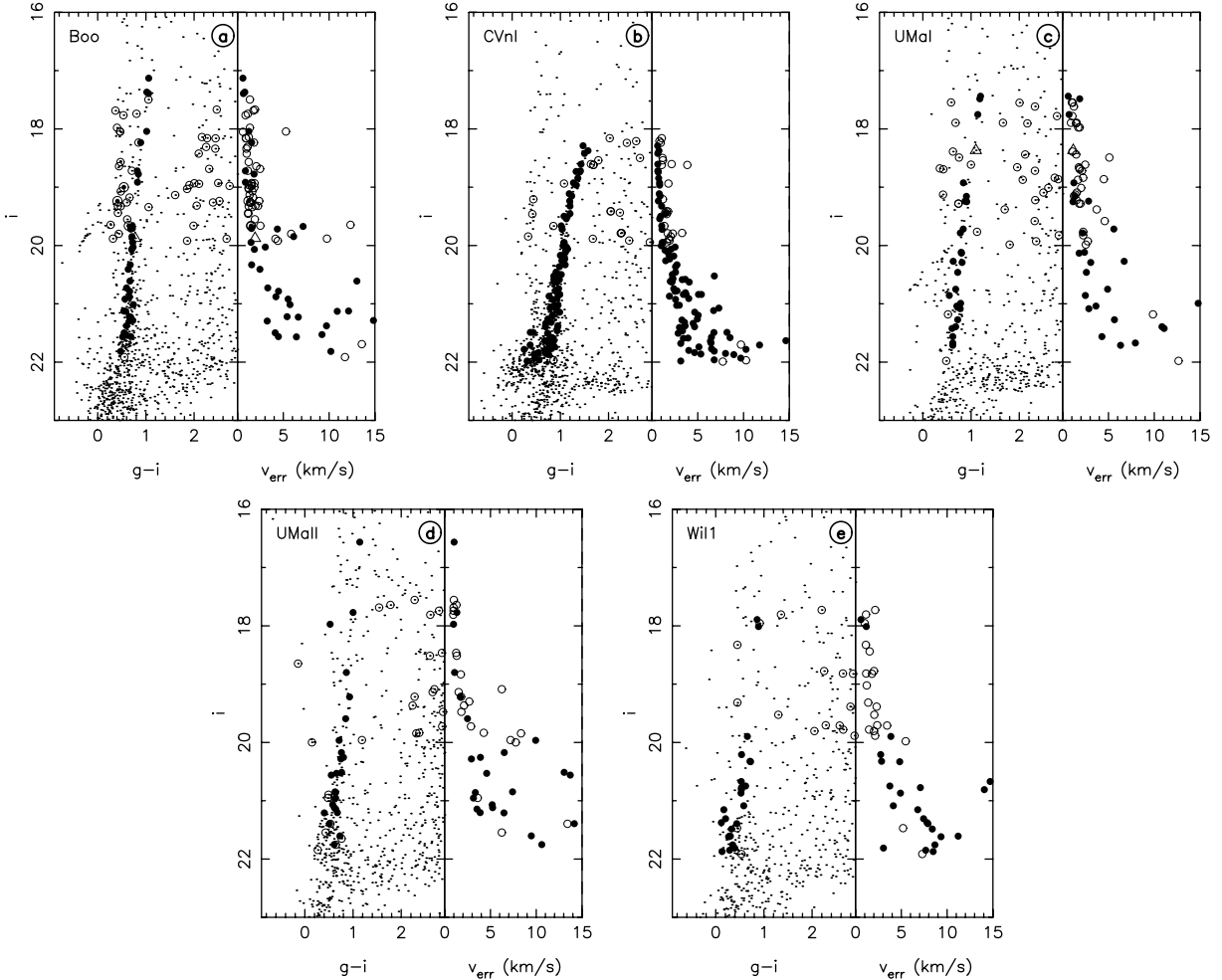**Figure 2.** SDSS CMDs within 10 arcmin of the centre of the satellites (left-hand panel of each figure) and radial velocity uncertainties of the observed stars in the five satellites in this survey (right-hand panel of each figure). As in Fig. 1, panel (a) corresponds to Boo, panel (b) to CVnI, panel (c) to UMaI, panel (d) to UMaII and panel (e) to Wil1. The symbols are the same as in Fig. 1.
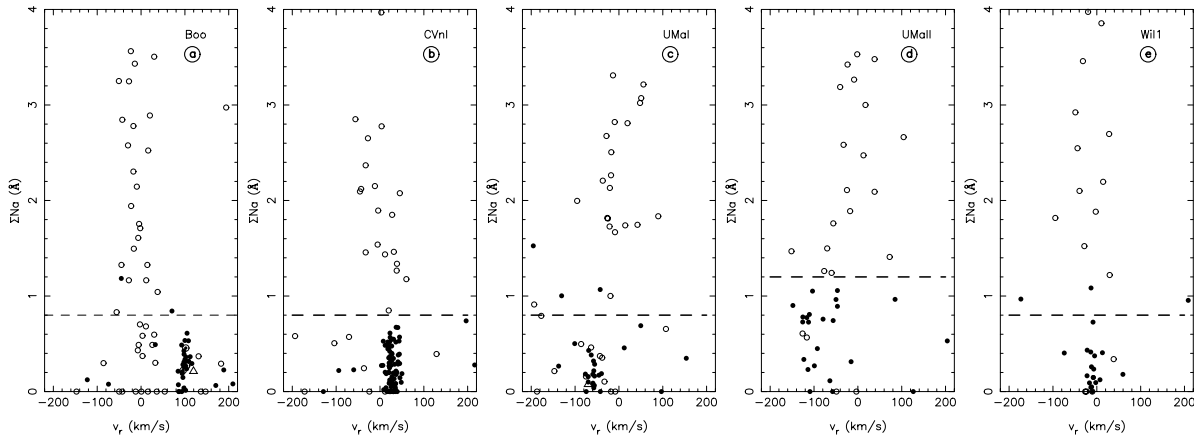
Figure 3. Distribution of the sodium doublet EW for the stars observed in each satellite. The symbols are the same as in Fig. 1 except for the filled circles that here represent the initial CMD selection of satellite members, prior to the ΣNa cut. Except in the case of UMaII, the difference between field stars and satellite members is directly visible and, as expected, giant stars (filled circles) have low ΣNa contrary to contaminating dwarfs. From these plots we derive the ΣNa $= 0.8$ Å cut we use to isolate genuine giants (in the case of UMaII, see Section 6 for more details).
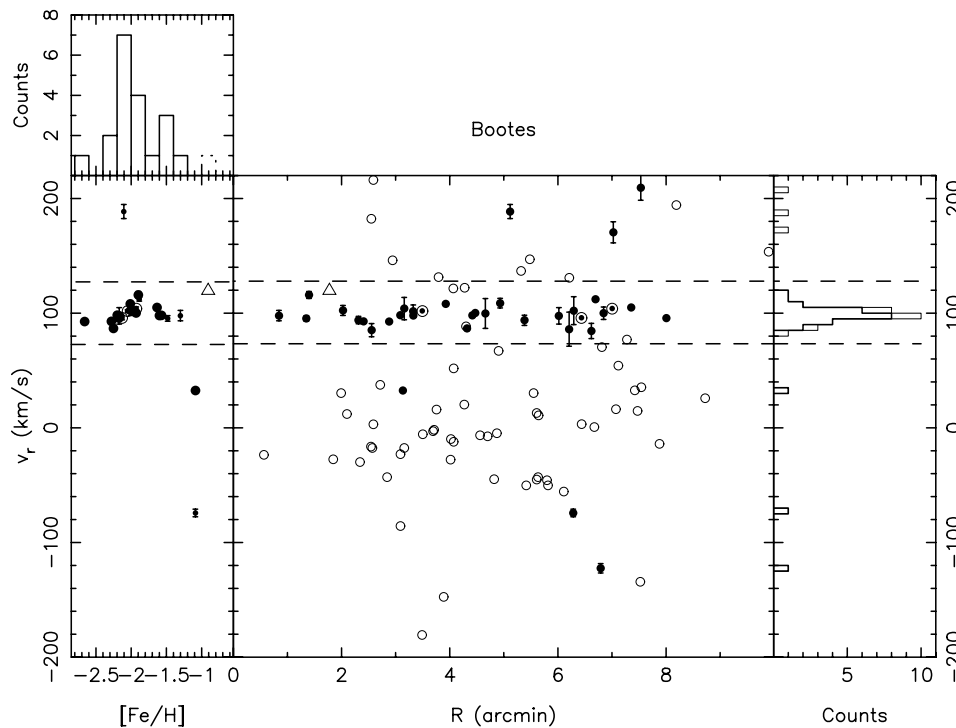
Figure 4. Summary of the spectroscopic DEIMOS observations of Boo. The central panel shows the radial velocity of each target star as a function of distance to the centre of the dwarf galaxy. Hollow circles are stars that were excluded by the gravity sensitive ΣNa cuts and are most likely foreground dwarf stars. Filled circles represent the most probable Boo members, that is, stars aligned along the dwarf RGBs that were not excluded by the ΣNa cut. The triangle also corresponds to an object within the CMD selection region but that is probably not a Boo member since it has a high metallicity ([Fe/H] > -1.0). The three field stars with Boo-like velocities are represented by circled big dots and are considered as Boo members since they are also located close to the CMD features of the dwarfs. The error bars represent the 1σ radial velocity uncertainties, those that are not shown are smaller than the symbols and lower than $\sim$5 km s^{-1}. The thin line in the right-hand panel represents the radial velocity distribution of the Boo members whereas the thick line is restricted to those stars with an uncertainty lower than 6 km s^{-1}. The bottom left-hand panel presents the metallicity distribution for these stars that also have S/N > 15 as big filled circles necessary to derive a reliable [Fe/H] value (with uncertainties of ± 0.2 dex) and these with $15 >$ S/N > 10 and less reliable [Fe/H] as smaller dots. There is no significant difference between the two subsamples. In the three bottom panels, the dashed lines correspond to the radial velocity limits that were used to isolate Boo star members (see the text for more details). The top left-hand panel represents the metallicity distribution of the Boo members, that is, stars that form the radial velocity peak. The dotted histogram includes the star that has [Fe/H] > -1.0 and that is probably not a member of the dwarf galaxy.

that is close to the Boo peak but is more metal-rich than the other Boo stars. An S/N of 21 makes it unlikely that its metallicity has high uncertainties. Other stars in the sample with [Fe/H] ~ -1.0 are clearly not Boo members, which also hints at a [Fe/H] value

that is not meaningful for this star. However, should later studies reveal that Boo contains such a metal-rich population, we will determine the velocity parameters of the dwarf with and without this star.

Table 1. Derived parameters for stars in the Boo sample.

α (J2000)	δ (J2000)	g	i	v_r (km s^{-1})	v_{err} (km s^{-1})	S/N (Å^{-1})	[Fe/H]	ΣCa (Å)	ΣNa (Å)	Member?
14 00 23.75	14 30 46.3	18.64	16.45	−45.7	1.0	73	–	3.6	2.2	n
13 59 41.24	14 33 09.4	17.98	17.39	−64.6	0.8	63	–	2.9	0.5	n
14 00 31.82	14 32 24.4	17.74	17.29	7.3	1.2	80	–	2.4	0.4	n
14 00 10.49	14 31 45.5	18.19	17.13	98.2	0.6	54	−2.2	2.3	0.4	y
14 00 12.92	14 33 11.8	19.54	18.72	100.1	0.9	41	−1.9	2.0	0.5	y
14 00 33.08	14 29 59.7	19.74	18.92	95.6	0.9	43	−2.2	1.3	0.3	y
14 00 22.97	14 30 45.0	18.55	17.50	−45.0	1.4	57	–	4.6	1.2	n
14 00 03.08	14 30 23.6	21.45	20.78	97.9	4.5	10	−1.3	2.3	0.0	y
14 00 24.62	14 31 59.6	21.33	20.73	−74.3	3.3	11	–	2.8	0.1	n
13 59 44.27	14 32 41.2	21.28	20.61	99.7	13.0	8	–	1.7	0.3	y
13 59 52.33	14 32 45.7	20.67	19.95	97.9	1.5	19	−1.6	2.1	0.4	y
13 59 53.76	14 30 56.0	20.65	19.88	119.6	1.9	21	–	3.8	0.2	n
14 00 05.34	14 30 23.3	21.04	20.41	95.4	2.5	11	−1.5	2.1	0.1	y
14 00 00.83	14 33 07.7	19.06	18.04	32.6	1.2	35	–	4.4	0.5	n
13 59 44.96	14 32 30.1	20.77	20.07	98.0	1.8	18	−1.6	2.1	0.3	y
14 00 15.42	14 32 08.5	22.28	21.69	−235.0	13.6	5	–	9.2	0.9	n
14 00 23.38	14 32 45.3	21.67	21.12	102.2	12.1	6	–	1.0	0.3	y
13 59 51.08	14 30 49.8	21.96	21.30	94.0	3.2	5	–	1.7	0.2	y
13 59 50.76	14 31 14.2	21.75	21.01	85.2	5.7	8	–	1.5	0.1	y
13 59 48.85	14 33 43.6	22.09	21.57	−443.4	6.4	3	–	0.6	0.0	n
14 00 12.25	14 31 51.9	18.52	18.05	−5.4	0.6	57	–	1.7	0.5	n
14 00 13.93	14 33 04.4	20.43	18.16	−6.5	0.9	52	–	3.1	1.6	n
14 00 17.14	14 33 48.6	19.86	19.44	−43.0	1.2	26	–	1.8	0.0	n
14 00 24.94	14 30 56.9	20.40	19.34	−55.5	1.6	27	–	4.7	0.8	n
14 00 27.29	14 32 19.6	20.31	19.66	103.9	1.5	25	−1.9	1.5	0.3	y
14 00 22.45	14 33 26.9	19.54	19.00	95.8	1.7	29	−2.1	1.5	0.2	y
14 00 25.71	14 34 15.4	20.56	18.31	35.5	1.1	48	–	3.3	0.0	n
14 00 06.98	14 32 07.8	18.55	17.74	37.5	1.1	57	–	4.2	1.0	n
14 00 28.73	14 31 18.2	20.78	18.34	16.2	1.0	51	–	2.8	2.5	n
14 00 07.35	14 31 51.1	20.61	18.16	−17.7	0.9	49	–	2.8	2.8	n
13 59 36.02	14 34 07.1	18.38	17.98	54.1	1.4	53	–	2.8	0.0	n
13 59 40.86	14 32 48.3	21.71	18.98	−50.2	1.5	32	–	1.7	3.2	n
14 00 29.72	14 31 50.0	20.16	19.55	32.6	1.9	24	–	3.6	0.3	n
13 59 45.95	14 31 40.6	19.91	19.65	131.3	12.3	24	–	4.7	0.4	n
13 59 48.34	14 32 03.6	19.65	19.24	101.9	1.2	30	−2.1	1.6	0.5	y
13 59 40.29	14 30 59.7	21.05	18.94	−4.8	1.5	36	–	3.4	1.8	n
13 59 31.58	14 32 55.3	20.74	19.14	14.6	1.3	33	–	3.7	1.3	n
13 59 33.58	14 30 44.6	19.80	19.33	3.2	1.2	30	–	3.0	0.4	n
14 00 05.67	14 33 29.8	21.64	19.66	15.9	2.5	25	–	3.4	0.0	n
14 00 08.99	14 33 26.6	21.38	19.32	−12.2	2.0	33	–	3.3	0.0	n
14 00 09.89	14 30 52.0	20.89	19.03	−16.5	1.2	35	–	3.8	1.5	n
14 00 04.87	14 31 44.2	21.78	19.92	12.0	4.4	15	–	3.3	1.2	n
13 59 39.84	14 34 33.4	19.42	18.72	0.8	1.1	36	–	1.7	0.0	n
13 59 56.61	14 32 43.3	21.76	19.24	−43.0	2.4	32	–	2.5	2.8	n
13 59 46.27	14 34 09.2	19.84	19.18	136.6	1.7	23	–	2.2	0.0	n
13 59 47.72	14 30 50.6	20.52	18.42	−22.9	1.0	46	–	3.3	1.9	n
13 59 48.04	14 31 16.3	20.30	18.14	−17.6	1.2	46	–	3.5	2.3	n
14 00 32.48	14 30 29.9	22.60	19.66	−13.9	1.4	29	–	1.5	3.4	n
14 00 04.61	14 31 28.1	22.39	19.45	−27.5	1.2	32	–	1.9	3.2	n
13 59 57.69	14 29 55.4	17.76	14.84	−23.5	2.0	48	–	1.8	3.6	n
13 59 43.83	14 32 48.8	20.86	18.96	−44.7	1.2	40	–	3.6	1.3	n
14 00 18.66	14 33 23.1	18.30	17.76	10.9	0.9	60	–	3.5	0.7	n
13 59 22.71	14 25 56.8	15.37	14.32	153.6	12.4	151	–	3.9	1.2	n
14 00 20.11	14 29 23.6	19.49	17.17	67.1	1.7	76	–	2.9	1.6	n
13 59 33.85	14 29 12.1	18.07	17.40	9.9	1.2	61	–	3.8	0.4	n
14 00 19.77	14 27 04.6	19.60	17.11	13.0	1.1	70	–	2.6	2.9	n
13 59 57.85	14 28 02.5	20.40	19.72	102.4	4.4	18	−2.0	1.3	0.4	y
13 59 39.37	14 26 38.4	20.38	19.67	97.6	7.2	21	−2.2	0.9	0.3	y
13 59 42.19	14 29 42.3	19.62	18.77	86.6	1.8	37	−2.3	1.2	0.0	y
14 00 03.33	14 28 51.5	20.76	20.03	115.9	3.0	18	−1.9	1.3	0.3	y
14 00 05.61	14 26 18.9	20.43	19.71	108.1	1.5	22	−2.0	1.3	0.5	y
13 59 47.07	14 28 52.6	21.48	20.92	101.6	5.5	8	–	1.7	0.0	y
14 00 09.85	14 28 23.0	18.45	17.39	92.6	0.6	60	−2.7	1.1	0.5	y

Table 1 – *continued*

α (J2000)	δ (J2000)	g	i	v_r (km s^{-1})	v_{err} (km s^{-1})	S/N (Å^{-1})	[Fe/H]	ΣCa (Å)	ΣNa (Å)	Member?
13 59 50.63	14 29 11.1	19.12	18.23	92.8	1.5	56	−2.3	1.5	0.0	y
14 00 11.54	14 25 56.1	21.54	20.88	108.7	4.2	9	–	1.4	0.3	y
14 00 25.83	14 26 07.6	18.38	17.37	104.9	0.8	48	−1.6	3.5	0.6	y
14 00 13.84	14 26 07.9	20.56	19.85	188.6	6.1	14	–	1.0	0.2	n
14 00 21.84	14 25 53.4	21.00	20.33	112.1	1.5	14	−1.9	1.2	0.4	y
14 00 26.18	14 27 29.5	19.08	18.24	70.4	1.8	41	–	3.7	0.8	n
13 59 33.51	14 28 21.6	21.91	21.23	84.4	6.6	6	–	2.1	0.2	y
13 59 34.38	14 30 17.2	22.02	21.29	86.0	14.8	5	–	0.3	0.0	y
13 59 32.07	14 27 12.5	22.46	21.91	−416.3	11.8	4	–	0.6	2.1	n
13 59 32.74	14 28 23.5	22.05	21.50	−122.5	4.1	5	–	2.2	0.1	n
14 00 02.29	14 26 53.4	21.97	21.38	104.0	9.7	7	–	1.2	0.2	y
13 59 45.71	14 25 52.6	22.25	21.56	93.8	4.5	5	–	12.4	0.2	y
14 00 01.73	14 26 16.2	22.29	21.82	239.4	10.2	4	–	2.3	0.4	n
14 00 28.70	14 27 05.2	21.71	21.13	209.3	10.9	6	–	1.4	0.1	n
14 00 23.34	14 26 08.0	21.87	21.22	99.9	5.4	7	–	2.2	0.3	y
14 00 25.04	14 26 27.0	22.11	21.53	170.4	9.2	5	–	0.1	0.1	n
14 00 22.78	14 29 20.5	18.51	18.05	30.2	5.3	52	–	2.2	0.6	n
14 00 15.97	14 30 24.8	18.05	17.69	−147.4	1.7	65	–	1.5	0.0	n
13 59 36.00	14 29 38.5	19.04	18.57	−50.1	1.2	39	–	2.6	0.0	n
13 59 26.54	14 26 45.3	19.08	18.64	25.8	2.0	33	–	2.3	0.5	n
13 59 26.24	14 29 29.2	22.56	19.88	194.1	4.2	12	–	3.0	3.0	n
13 59 37.39	14 29 41.6	20.94	18.93	147.1	1.9	36	–	3.7	0.0	n
13 59 45.17	14 29 03.9	20.14	17.67	−1.7	1.9	55	–	2.7	1.7	n
14 00 04.12	14 27 36.7	19.74	19.32	3.1	2.2	26	–	2.2	0.6	n
14 00 04.62	14 26 08.4	21.66	19.26	−9.8	1.4	30	–	3.1	2.1	n
13 59 49.62	14 28 12.0	20.24	19.80	−85.6	5.9	17	–	2.4	0.3	n
14 00 10.26	14 26 00.4	19.86	19.26	−7.4	1.4	27	–	1.7	0.4	n
13 59 43.92	14 29 00.0	21.43	18.93	−27.9	1.6	35	–	2.6	1.2	n
13 59 52.16	14 28 37.7	21.00	18.68	−29.9	2.5	38	–	2.8	2.6	n
13 59 50.91	14 28 42.6	20.20	19.88	182.2	9.8	16	–	44.4	0.3	n
14 00 06.65	14 28 49.6	21.92	19.01	30.2	1.2	32	–	1.8	3.5	n
14 00 14.85	14 29 09.6	19.55	19.07	−2.8	1.6	27	–	2.2	0.7	n
14 00 15.18	14 27 49.8	17.98	15.67	20.2	1.9	60	–	3.0	2.9	n

Columns (1) and (2) correspond to the J2000 coordinates of the stars as they appear in SDSS. Columns (3) and (4) are the *g* and *i* magnitudes observed by the SDSS. Columns (5) and (6) are the measured radial velocity and the corresponding uncertainty. Column (7) is the S/N of the spectrum, Column (8) is the derived metallicity of Boo members with S/N > 10 Å^{-1}, Column (9) is the weighted sum of the EWs of the three Ca I lines at 8498, 8542 and 8662 Å, Column (10) is the sum of the EWs of the two Na I lines at 8193 and 8195 Å and Column (11) has the value 'y' for stars that were used to derive the parameters of the dwarf. None-members ('n' value) have v_{err} > 15 km s^{-1}, are aligned with the Boo CMD features, have [Fe/H] > −1.0, have ΣNa > 0.8 or are clearly away from the radial velocity peak produced by the dwarf galaxy.

Using only the confirmed Boo stars, we iteratively determine the mean radial velocity, v_r, and velocity dispersion, σ, of the dwarf galaxy by clipping stars within $\pm 3\sigma$ of v_r and determine anew the mean radial velocity and the velocity dispersion of the sample defined in this way. After each iteration, the best parameters are determined with a maximum likelihood algorithm that explores a coarse grid of the (v_r, σ) space and searches for the couple of parameters that maximizes the maximum likelihood (ML) function defined as

$$ML(v_r, \sigma) = \sum_{i=1}^{N} \frac{1}{\sigma_{tot}} \exp\left[-\frac{1}{2}\left(\frac{v_r - v_{r,i}}{\sigma_{tot}}\right)^2 \right] \quad (1)$$

with *N* the number of stars in the sample, $\sigma_{tot} = \sqrt{\sigma^2 + v_{err,i}^2}$, $v_{r,i}$ the radial velocity measured for the *i*th star and $v_{err,i}$ the corresponding uncertainty. Using this definition of σ_{tot} allows us to disentangle the intrinsic velocity dispersion of the dwarf galaxy population, σ, and the contribution of the measurement uncertainties to the observed distribution. By definition, this technique also gives a low weight to stars with poorly determined radial velocity and is therefore applicable to the whole velocity sample without removing those stars that have a high velocity uncertainty.

Starting values are taken from Muñoz et al. (2006, $v_r = 95.6$ km s^{-1} and $\sigma = 6.6$ km s^{-1}) and convergence is achieved for $v_r = 99.0 \pm 2.1$ km s^{-1} (or $v_{gsr} = 106.5 \pm 2.1$ km s^{-1}) and $\sigma = 6.5^{+2.0}_{-1.4}$ km s^{-1} determined with a final sample of 30 stars. This is in good agreement with but more precise than the value of Muñoz et al. (2006) determined from only seven stars. Restricting the sample to the 24 stars with $v_{err} < 6$ km s^{-1} (the thick line in the right-hand panel of Fig. 4)[2] to ensure that the individual uncertainties do not influence the convergence, the derived parameters are statistically equivalent ($\sigma = 6.5^{+2.1}_{-1.3}$ km s^{-1} and $v_r = 99.9 \pm 2.4$ km s^{-1}). With this quality cut, the radial velocity distribution that is represented by the thick line in the right-hand panel of Fig. 4 shows a very clear peak. In all cases, the stars that are removed by the 3σ clipping all have radial velocity that are clearly different from the systemic velocity of Boo. Adding the metal-rich star yields a slightly higher velocity dispersion $\sigma = 7.4^{+2.2}_{-1.2}$ km s^{-1} centred on $v_r = 99.8 \pm 2.4$ km s^{-1}.

[2] The 6-km s^{-1} threshold is a good compromise between the quality of the individual velocity values and the number of stars in the sample.

As is usually done for dwarf galaxies, one can try to estimate the mass of Boo from its central velocity dispersion, and structural parameters, assuming it is a spherical system in virial equilibrium. Even though it may not be the case, the central velocity dispersion can still be used to measure the instantaneous mass content of the structure (e.g. Oh et al. 1995; Piatek & Pryor 1995). The Richstone & Tremaine (1986) formula can be used to derive the M/L of the system in solar units:

$$M/L = \eta \frac{9}{2\pi G} \frac{\sigma_0^2}{S_0 r_{hb}}, \qquad (2)$$

where η is a scale parameter close to 1.0, S_0 is the central surface brightness of the dwarf, r_{hb} its half-light radius and σ_0 its central velocity dispersion. Alternatively, the Illingworth (1976) approach directly gives the mass M of the system in solar units:

$$M = 167 \, r_c \, \mu \, \sigma_0^2 \qquad (3)$$

with r_c the core radius of the system in parsecs and μ a scalefactor taken as 8 by Mateo (1998). Both methods are not highly accurate since for equation (2), S_0 can have uncertainties of $\sim$50 per cent for the faint systems considered here and determining the mass requires using the luminosity of the system, itself not well constrained (see e.g. Muñoz et al. 2006). Equation (3) should yield a better mass estimate since it does not require the (poorly constrained) luminosity of the satellites as an input parameter but it relies on the core radius r_c of the systems, which have not been determined with accuracy for the satellites studied in this paper. Following Muñoz et al. (2006), we use the approximation $r_c \sim r_{hb}$ which is usually reliable within ± 25 per cent although there are some dwarf galaxies which show sizable difference between r_c and r_{hb} (see e.g. McConnachie & Irwin 2006).

Applying equation (2) for Boo with $\sigma_0 = \sigma = 6.5 \, \text{km s}^{-1}$, $S_0 \sim 0.20 \, \text{L}_\odot \, \text{pc}^{-2}$ derived from the exponential profile of the dwarf determined by Belokurov et al. (2006a) yields $(M/L) = 220$ in solar units. Assuming $L = 1.8 \times 10^4 \, \text{L}_\odot$ ($M_V = -5.8$) then yields a total mass of $M \sim 4 \times 10^6 \, \text{M}_\odot$ although if we follow Muñoz et al. (2006) and use the brighter $L = 8.6 \times 10^4 \, \text{L}_\odot$ ($M_V = -6.75$) we obtain $M \sim 1.8 \times 10^7 \, \text{M}_\odot$. On the other hand, equation (3) yields $M \sim 1.3 \times 10^7 \, \text{M}_\odot$, obviously in agreement with Muñoz et al. (2006) since the velocity dispersion we use is very similar to theirs.

Boo is close enough to the Milky Way that a significant portion of the observed stars have a high enough S/N to allow for a proper determination of their metallicity. The metallicity distribution of the most probable Boo stars is presented on the bottom left-hand panel of Fig. 4 with the values derived from the highest quality spectra (S/N > 15 or 0.2 dex uncertainty on [Fe/H]) as the bigger filled circles and lower quality spectra (15 > S/N > 10) as smaller filled circles. There is no significant difference in the distribution of these two subsamples and we therefore merge them together to study the metallicity of Boo. Isolating stars in the velocity peak yields the distribution of the top left-hand panel and confirms Boo is a metal-poor satellite of the Milky Way, though somewhat less metal-poor than was measured in previous studies based on isochrone fitting with SDSS photometry ([Fe/H] ~ -2.3; Belokurov et al. 2006a), a combined spectrum of seven confirmed Boo stars ([Fe/H] ~ -2.5; Muñoz et al. 2006) or RR Lyrae ([Fe/H] ~ -2.5; Siegel (2006). The median metallicity derived from the DEIMOS sample is indeed [Fe/H] = -2.1, though one star is as metal-poor as [Fe/H] = -2.7. It is unclear why the value is more metal-rich than previous estimates. A comparison with metallicities determined photometrically by comparison of the RGB stars with the 10-Gyr isochrones from Girardi et al. (2004) shows only a tiny systematic shift to more metal-rich values of 0.1 dex (in agreement with

the Belokurov et al. 2006a, photometric metallicity estimate) but this shift could also be due to the age assumed for the isochrones. The discrepancy in the metallicity may also be related to the Carretta & Gratton (1997) metallicity scale used here compared to the Zinn & West (1984) scale used by Siegel (2006). Fig. 5 of Carretta & Gratton (1997) points out that the Zinn & West scale is always ~ 0.1 dex more metal-poor than the Carretta & Gratton (1997) scale for [Fe/H] $\lesssim -2.0$ which bridges part of the discrepancy with the Siegel (2006) values. Finally, since none of these systematics are large enough to account for the 0.5 dex difference between our value and those measured by Muñoz et al. (2006) and Siegel (2006), it has to be noted that none of the techniques used to estimate [Fe/H] have been calibrated for [Fe/H] $\lesssim -2.3$. The extrapolated relations used in all these studies (including ours) could therefore start diverging at the low metallicity of Boo.

4 CANES VENATICI I

Discovered in the SDSS by Zucker et al. (2006a), CVnI is the furthest of the newly discovered Milky Way faint dwarf galaxies with a heliocentric distance of $\sim$220 kpc. It is also the brightest, with $M_V = -7.9 \pm 0.5$, making it a galaxy similar to the Draco dSph, but with a bigger physical size (half-light radius $r_{hb} \sim 550$ pc). The populated RGB of this satellite (see Fig. 2b) makes it a perfect target for DEIMOS and we were able to observe 127 stars with two pointings. An analysis of this dwarf galaxy is presented in details in Ibata et al. (2006) and reveals that CVnI hosts two distinct stellar populations: one is metal-poor ($-2.5 \lesssim$ [Fe/H] $\lesssim -2.0$), kinematically hot ($\sigma = 13.9^{+3.2}_{-2.5} \, \text{km s}^{-1}$) and extended ($r_{hb} = 7.8^{+2.4}_{-2.1}$ arcmin) while the second one is concentrated at the centre of the dwarf ($r_{hb} = 3.6^{+1.1}_{-0.8}$ arcmin), is more metal-rich ($-2.0 \lesssim$ [Fe/H] $\lesssim -1.5$) and has a near-zero velocity dispersion (with a dispersion lower than 1.9 km s^{-1} at the 99 per cent confidence level). Though there is growing evidence that many dwarf galaxies harbour kinematically and structurally distinct populations or at least population gradients (see e.g. Harbeck et al. 2001; Tolstoy et al. 2004 for Sculptor; Battaglia et al. 2006 for Fornax), CVnI is to date the most extreme case of such a behaviour. It is also the first time that a near-zero velocity dispersion is discovered in a dwarf galaxy though deeper observations are required before putting strong constraints on the dark matter content of this dwarf galaxy.

We nevertheless reproduce Fig. 4 for the CVnI dwarf in Fig. 5 for comparison and list the characteristics of the observed stars in Table 2.

5 URSA MAJOR I

UMaI was discovered by Willman et al. (2005b) from an automatic search of faint substructures in the SDSS. Though the parameters of this satellite are not well constrained given the low number of stars on its RGB and the absence of deep observations that reach the more populated main-sequence turn-off, UMaI appears to be at a distance of $\sim$100 kpc, with $M_V \sim -6.75$, $r_{hb} = 250$ pc and a metallicity roughly estimated to be within $-2.1 \lesssim$ [Fe/H] $\lesssim -1.7$. Kleyna et al. (2005) observed seven stars near the tip of the RGB with the High Resolution Echelle Spectrometer (HIRES) spectrograph mounted on the Keck I telescope and concluded that five of these are likely members of the galaxy. They derive a mean systemic velocity of $v_r = -52.4 \pm 4.3 \, \text{km s}^{-1}$ and a velocity dispersion of $\sigma = 9.3^{+11.7}_{-1.2} \, \text{km s}^{-1}$ through a maximum likelihood algorithm and subsequently use these values to infer an M/L of the order of $\sim$500 in solar units for UMaI.
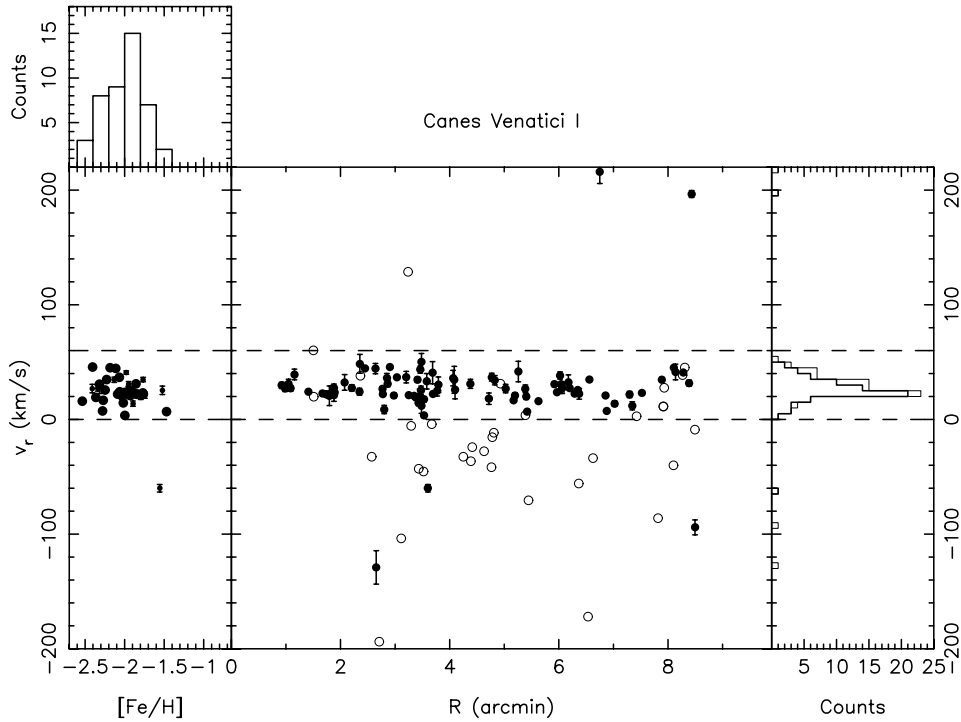
Figure 5. Same as Fig. 4 for the CVnI dwarf galaxy.

To increase the number of observed stars in the dwarf galaxy, two DEIMOS fields were observed at the centre of UMaI, roughly covering the region within the half-light radius of the dwarf (Fig. 1c). As before, Fig. 2(c) shows the CMD taken from the SDSS for this region of the sky along with the selected targets and the Na I doublet discrimination is presented Fig. 3(c). The parameters of the observed stars are listed in Table 3. Two of our stars were observed by Kleyna et al. (2005) with the HIRES spectrograph on Keck (their stars 1 and 7). The shift between the two measurements of star 1 is small ($2.3 \, \mathrm{km \, s^{-1}}$) whereas star 7 shows a shift of $13.1 \, \mathrm{km \, s^{-1}}$, but this is probably due to the high uncertainty of the HIRES value ($>5 \, \mathrm{km \, s^{-1}}$) since the DEIMOS observation has an uncertainty of only $1.2 \, \mathrm{km \, s^{-1}}$. As there are only three stars in their sample that were not re-observed with DEIMOS, we prefer not to add them to our ~17 stars that fall in the velocity range of UMaI to avoid adding a source of systematics.

Contrary to Boo, UMaI has a velocity distribution that overlaps with the Galactic contaminants (Fig. 6). The dwarf galaxy stars, however, seem to produce a very narrow peak of eight stars surrounded by a broader group of stars for which it is difficult to definitely conclude whether they belong to UMaI or to the Galactic contamination (only one star is removed from the sample since, with a metallicity of $[\mathrm{Fe/H}] = -0.8$, it is inconsistent with the metal-poor population of the dwarf and is hence most probably a dwarf stars for which the determined $[\mathrm{Fe/H}]$ has no meaningful sense). Applying the maximum likelihood technique that was applied on the Boo sample yields a systemic velocity of $v_r = -57.0 \pm 3.5 \, \mathrm{km \, s^{-1}}$ and a velocity dispersion $\sigma = 11.9^{+3.5}_{-2.3} \, \mathrm{km \, s^{-1}}$ for the stars aligned along the CMD features of the dwarf, in good agreement with the Kleyna et al. (2005) measurement.[3] A Kolmogorov–Smirnov test between

the 17 stars used for this best fit and the fit itself, however, only gives a probability of 19 per cent that the data follow the fit distribution. With this in mind, it is interesting to note that the narrow peak of the velocity distribution at $v_r \sim 57 \, \mathrm{km \, s^{-1}}$ is reminiscent of the very low velocity dispersion peak observed in CVnI (Ibata et al. 2006). This is also of particular interest since some of the more broadly distributed objects may only be Galactic contaminants as is hinted at by the higher metallicity of the two stars at higher velocity than the peak ($[\mathrm{Fe/H}] \sim -1.5$). As for CVnI, this narrow peak is compatible with a dispersion of $0 \, \mathrm{km \, s^{-1}}$. It also has a dispersion that is lower than $3.4 \, \mathrm{km \, s^{-1}}$ at the 99 per cent confidence level.

One can nevertheless use the derived dispersion values to put some constraints on the M/L of UMaI. Since no central surface brightness value S_0 has been measured for UMaI, Kleyna et al. (2005) has assumed a uniform luminosity distribution within the half-light radius of the galaxy; this yields $S_0 = 0.11 \, \mathrm{L_\odot \, pc^{-2}}$ and is certainly a lower limit to S_0 given that dwarf galaxies have peaked luminosity profiles. Indeed, reproducing this estimate for the Boo galaxy yields the same value whereas the central surface brightness of this galaxy is measured to be $S_0 = 0.20 \, \mathrm{L_\odot \, pc^{-2}}$ when using the central surface brightness measured by Belokurov et al. (2006a, see Section 4). Hence, we prefer using $S_0 \sim 0.20 \, \mathrm{L_\odot \, pc^{-2}}$ for UMaI and, along with $\sigma = 11.9 \, \mathrm{km \, s^{-1}}$ and $r_{hb} = 250 \, \mathrm{pc}$, we derive $(M/L) \sim 900 \, \mathrm{M_\odot / L_\odot}$ using equation (2). With $L \sim 4.3 \times 10^4 \, \mathrm{L_\odot}$, this converts to $M \sim 3.8 \times 10^7 \, \mathrm{M_\odot}$. Alternatively, $M = 4.7 \times 10^7 \, \mathrm{M_\odot}$ can be derived from equation (3). These estimates make UMaI a highly dark matter dominated dwarf galaxy. However, as was shown by Ibata et al. (2006) in the analysis of CVnI, deriving the total mass of the system may not be straightforward if the dwarf galaxy hosts more than one stellar component. If we were to use only the stars in the narrow peak of UMaI, the total mass of the system would be lower than $3.8 \times 10^6 \, \mathrm{M_\odot}$ at the 99 per cent confidence limit through equation (3), a drastically dissimilar value that urges for a larger sample of high-accuracy radial velocities. This could be

---

[3] Including the metal-rich star leads to a systemic velocity $v_r = -59.1 \pm 4.1 \, \mathrm{km \, s^{-1}}$ and a velocity dispersion $\sigma = 12.8^{+3.6}_{-2.5} \, \mathrm{km \, s^{-1}}$.

Table 2. Derived parameters for stars in the CVnI sample.

α (J2000)	δ (J2000)	g	i	v_r (km s^{-1})	v_{err} (km s^{-1})	S/N (Å^{-1})	[Fe/H]	ΣCa (Å)	ΣNa (Å)	Member?
13 27 33.02	33 37 54.5	17.26	16.57	−86.1	1.0	62	−	4.1	1.4	n
13 28 25.01	33 34 58.9	19.77	17.27	−41.7	1.2	40	−	2.8	2.4	n
13 28 41.21	33 36 34.2	19.76	16.80	−8.9	2.0	47	−	1.6	3.8	n
13 27 27.51	33 36 25.0	18.27	16.51	−40.0	1.0	63	−	4.5	1.6	n
13 27 36.41	33 37 16.8	19.76	18.29	7.5	0.6	56	−2.3	2.9	0.5	y
13 27 49.42	33 38 09.0	21.03	19.95	15.9	1.2	18	−2.5	1.4	0.0	y
13 28 13.74	33 35 55.6	20.20	18.93	20.7	0.8	32	−2.0	3.1	0.3	y
13 28 28.27	33 37 02.8	20.03	18.60	25.5	0.6	42	−2.2	2.8	0.3	y
13 28 27.56	33 36 43.2	19.92	18.42	30.6	0.6	42	−2.3	2.7	0.3	y
13 28 07.83	33 36 38.3	21.45	20.57	34.6	2.3	12	−2.1	2.0	0.0	y
13 27 58.61	33 36 54.0	20.20	18.84	22.3	0.7	40	−1.8	3.8	0.5	y
13 28 10.82	33 36 31.9	21.23	20.18	17.5	2.4	9	−	2.7	0.5	y
13 28 20.95	33 38 04.8	20.14	18.74	23.6	0.7	41	−1.9	3.5	0.0	y
13 28 20.63	33 38 04.3	21.51	20.61	30.8	2.2	12	−1.9	2.4	0.0	y
13 28 21.84	33 38 41.0	20.14	18.72	34.8	0.6	49	−2.2	2.7	0.0	y
13 28 02.64	33 36 06.8	21.52	20.61	26.7	2.0	13	−1.9	2.5	0.1	y
13 28 29.71	33 36 28.6	21.52	20.50	22.5	2.2	11	−2.0	2.2	0.4	y
13 28 39.76	33 35 37.2	21.64	20.87	34.8	1.9	13	−1.8	2.7	0.1	y
13 28 17.67	33 35 11.0	21.76	20.81	25.4	3.7	12	−1.5	3.3	0.0	y
13 27 57.78	33 35 56.3	21.84	20.91	36.1	4.0	9	−	2.4	0.5	y
13 27 49.74	33 34 09.5	21.55	20.63	20.9	2.2	11	−1.8	2.8	0.3	y
13 27 34.95	33 34 30.6	21.80	20.84	27.7	5.1	10	−2.3	1.4	0.1	y
13 27 30.41	33 35 44.3	21.67	20.78	21.7	2.7	13	−1.8	2.7	0.1	y
13 27 59.57	33 34 03.9	21.72	20.79	27.2	2.5	11	−2.3	2.3	0.4	y
13 28 16.06	33 34 53.2	21.02	19.95	36.7	1.1	23	−2.1	2.5	0.2	y
13 28 26.79	33 34 39.7	21.45	20.58	26.9	3.6	11	−2.4	1.3	0.3	y
13 28 11.71	33 34 07.8	21.82	20.84	27.4	3.4	9	−	2.6	0.1	y
13 27 56.03	33 34 25.5	21.06	20.00	23.5	1.0	20	−2.0	2.6	0.3	y
13 27 34.01	33 36 23.8	21.19	20.08	20.8	1.4	17	−1.9	2.7	0.2	y
13 28 10.35	33 34 27.7	20.67	19.54	22.2	0.8	30	−1.8	3.3	0.4	y
13 27 51.59	33 35 43.2	21.16	20.03	14.4	2.5	17	−2.0	2.5	0.2	y
13 28 08.82	33 34 41.2	20.43	19.24	21.9	0.7	33	−2.1	2.8	0.2	y
13 27 47.82	33 36 54.2	22.49	21.80	34.2	4.0	5	−	2.6	0.1	y
13 28 00.00	33 36 28.2	22.03	21.20	36.9	5.0	7	−	2.8	0.2	y
13 28 04.85	33 35 58.5	22.03	21.34	44.3	4.5	9	−	2.3	0.4	y
13 28 22.77	33 36 44.7	22.63	21.87	41.7	8.9	5	−	2.7	0.4	y
13 28 38.38	33 34 25.7	22.13	21.32	11.9	3.6	7	−	1.7	0.2	y
13 28 34.77	33 35 07.1	22.03	21.78	215.9	10.3	3	−	4.0	0.3	n
13 28 16.48	33 37 16.9	22.44	21.59	36.8	3.4	6	−	2.4	0.7	y
13 28 00.83	33 36 05.6	22.33	21.38	8.6	3.6	7	−	2.1	0.0	y
13 27 57.16	33 36 34.4	22.53	21.77	11.8	6.5	5	−	61.1	0.5	y
13 27 35.36	33 35 17.5	22.43	21.67	32.4	6.4	5	−	3.2	0.1	y
13 27 37.37	33 35 55.6	22.29	21.98	38.3	3.2	4	−	6.4	0.2	y
13 27 52.51	33 35 47.4	22.03	21.28	229.7	3.3	6	−	1.9	0.3	n
13 28 05.88	33 34 12.0	22.24	21.50	27.1	2.8	8	−	3.3	0.1	y
13 28 09.55	33 34 43.2	22.62	21.74	24.6	5.1	7	−	2.8	0.3	y
13 28 08.50	33 34 26.4	22.83	21.97	19.9	10.3	4	−	5.6	0.8	n
13 27 54.82	33 34 22.1	22.52	21.96	32.3	6.8	5	−	1.7	0.2	y
13 28 14.08	33 34 12.6	22.34	21.70	38.0	9.7	4	−	2.9	1.3	n
13 27 38.84	33 37 06.5	20.78	18.21	−55.8	0.8	51	−	3.0	2.9	n
13 27 44.25	33 38 30.6	20.01	18.94	−172.0	1.8	37	−	3.9	0.0	n
13 27 53.03	33 36 00.2	20.62	18.24	−43.0	1.0	44	−	2.9	2.1	n
13 28 13.43	33 35 40.7	20.52	19.67	−103.9	1.4	26	−	4.0	0.5	n
13 28 19.25	33 35 00.1	20.18	18.16	−4.2	1.1	55	−	3.6	1.9	n
13 28 14.67	33 35 41.0	21.46	19.41	−5.7	1.6	28	−	4.0	1.5	n
13 28 06.29	33 35 59.9	19.65	19.21	−193.9	1.2	28	−	2.3	0.6	n
13 28 12.01	33 37 12.6	21.15	18.50	−32.5	1.2	43	−	2.4	2.4	n
13 27 29.49	33 35 34.4	22.92	19.80	2.9	2.3	28	−	1.8	4.0	n
13 27 24.40	33 34 45.9	20.33	18.54	38.8	1.2	49	−	3.6	1.3	n
13 27 25.64	33 34 01.9	20.30	18.62	11.2	3.8	54	−	3.8	1.4	n
13 28 28.99	33 34 34.0	21.56	19.89	−70.6	1.9	24	−	3.2	0.6	n
13 27 42.31	33 34 44.6	18.21	15.82	−27.6	1.8	53	−	3.2	2.7	n
13 27 19.95	33 32 08.0	16.82	16.34	−52.1	3.4	77	−	4.1	0.5	n
13 28 33.33	33 31 02.7	19.06	17.32	−33.7	1.3	71	−	4.6	1.6	n

© 2007 The Authors. Journal compilation © 2007 RAS, MNRAS **380**, 281–300

Table 2 – *continued*

α (J2000)	δ (J2000)	g	i	v_r (km s^{-1})	v_{err} (km s^{-1})	S/N (Å^{-1})	[Fe/H]	ΣCa (Å)	ΣNa (Å)	Member?
13 28 19.72	33 29 58.0	18.82	16.58	−15.6	0.9	66	–	3.6	2.3	n
13 27 18.23	33 29 50.5	18.12	16.50	−9.5	1.5	111	–	3.3	1.8	n
13 27 28.41	33 29 46.6	21.39	20.52	41.3	6.8	5	–	2.7	0.3	y
13 27 34.95	33 34 30.6	21.80	20.84	27.7	3.7	7	–	22.0	0.0	y
13 27 30.36	33 32 04.4	21.45	20.56	13.8	2.2	13	−1.9	2.6	0.0	y
13 27 24.86	33 31 25.0	21.29	20.26	40.9	1.5	15	−2.0	2.5	0.3	y
13 27 24.16	33 31 34.3	21.76	20.92	31.7	2.6	9	–	2.6	0.1	y
13 28 08.49	33 33 29.4	21.49	20.63	31.0	4.1	8	–	2.2	0.0	y
13 27 27.05	33 30 30.7	20.76	19.72	45.0	1.1	22	−2.2	2.4	0.3	y
13 27 39.32	33 32 05.0	21.70	20.74	20.8	2.4	11	−1.7	2.8	0.1	y
13 28 12.83	33 30 44.7	20.38	19.15	21.3	0.9	31	−1.9	3.3	0.3	y
13 28 16.23	33 34 09.9	20.66	19.45	22.0	1.5	30	−2.0	3.0	0.0	y
13 28 26.82	33 30 59.4	21.37	20.46	20.0	2.6	11	−1.8	2.9	0.2	y
13 28 28.78	33 32 04.3	21.22	20.06	6.7	2.1	22	−1.5	3.8	0.3	y
13 28 11.32	33 32 59.2	21.33	20.23	22.7	1.9	12	−1.9	2.7	0.6	y
13 28 17.15	33 33 42.5	21.35	20.36	31.1	2.6	16	−1.9	2.7	0.0	y
13 28 16.61	33 31 00.2	21.56	20.59	−60.0	3.3	15	–	3.3	0.2	n
13 28 18.51	33 31 42.6	21.17	20.17	3.5	1.9	17	−2.0	2.5	0.3	y
13 28 11.71	33 34 07.8	21.82	20.84	21.2	5.4	7	–	3.4	0.0	y
13 27 38.76	33 32 55.3	20.52	19.32	16.8	1.0	33	−2.3	2.3	0.5	y
13 28 01.41	33 30 00.1	20.30	19.11	19.2	0.8	38	−2.4	2.3	0.5	y
13 27 55.76	33 32 42.2	20.30	18.96	21.9	0.8	39	−1.8	3.5	0.5	y
13 27 31.21	33 29 59.2	19.95	18.38	23.1	0.8	52	−1.8	4.0	0.6	y
13 27 33.80	33 32 57.3	21.22	20.12	27.2	1.8	15	−2.0	2.6	0.2	y
13 28 10.07	33 33 41.6	20.68	19.66	24.1	1.1	25	−2.1	2.7	0.0	y
13 28 07.21	33 30 33.0	20.58	19.50	45.6	1.0	28	−2.4	2.0	0.1	y
13 28 08.19	33 31 06.3	20.06	18.73	44.5	0.7	42	−2.1	3.1	0.6	y
13 27 59.22	33 33 06.7	21.43	20.33	29.8	2.7	10	–	3.0	0.0	y
13 27 47.02	33 32 54.0	22.52	21.68	43.5	3.2	5	–	3.2	0.5	y
13 27 42.82	33 30 07.0	22.40	21.46	26.7	3.3	5	–	2.3	0.5	y
13 27 33.04	33 32 45.8	22.13	21.14	22.3	4.7	6	–	1.5	0.1	y
13 27 49.23	33 31 32.1	21.86	21.07	50.2	7.3	9	–	1.3	0.2	y
13 27 43.86	33 31 00.0	22.00	21.26	18.1	5.0	9	–	1.6	0.4	y
13 27 54.14	33 30 20.8	22.04	21.12	33.3	6.7	8	–	2.8	0.3	y
13 27 59.50	33 32 06.1	22.43	21.99	60.2	7.8	3	–	19.6	1.2	n
13 27 23.82	33 31 23.8	22.37	21.57	−94.1	6.5	4	–	5.2	0.2	n
13 28 02.45	33 31 09.2	21.91	21.03	27.5	2.7	9	–	2.9	0.4	y
13 28 03.24	33 30 06.4	22.32	21.86	233.6	5.3	4	–	3.6	0.1	n
13 27 23.12	33 32 45.7	22.34	21.41	196.6	3.0	4	–	10.5	0.7	n
13 28 08.96	33 33 08.5	22.38	21.84	39.2	4.7	4	–	2.2	0.0	y
13 27 48.31	33 30 46.1	22.08	21.71	34.5	11.8	5	–	2.4	0.0	y
13 27 50.23	33 29 57.2	22.41	21.59	31.0	3.9	5	–	1.9	0.5	y
13 27 51.73	33 30 35.8	22.40	21.93	40.7	9.7	4	–	3.8	0.7	y
13 27 52.99	33 30 16.7	22.09	21.40	25.1	4.7	8	–	1.9	0.1	y
13 28 03.54	33 29 54.1	22.34	21.64	20.1	6.4	5	–	2.5	0.4	y
13 28 04.59	33 31 00.4	21.87	21.49	48.5	8.2	6	–	51.6	0.1	y
13 28 12.11	33 33 14.9	22.41	21.58	20.6	8.5	4	–	4.4	0.0	y
13 28 19.11	33 31 23.8	22.54	21.81	30.3	6.8	4	–	4.9	0.2	y
13 28 13.25	33 29 49.9	21.93	21.49	36.0	6.8	7	–	2.6	0.1	y
13 28 23.11	33 33 01.0	22.54	21.85	26.0	8.0	6	–	4.2	0.5	y
13 28 14.66	33 33 40.6	21.98	21.02	24.2	3.0	7	–	2.8	0.0	y
13 28 15.56	33 34 12.3	22.31	21.63	−129.0	14.6	5	–	2.5	0.0	n
13 27 29.58	33 29 45.0	22.04	19.79	27.6	1.7	26	–	3.6	1.9	n
13 27 27.69	33 29 41.8	22.06	19.78	45.3	3.3	22	–	3.2	2.1	n
13 27 25.64	33 34 01.9	20.30	18.62	11.5	1.1	48	–	4.2	0.0	n
13 28 14.98	33 32 24.6	21.46	19.42	−32.6	1.8	29	–	3.5	1.5	n
13 28 26.07	33 32 20.7	21.67	19.44	−11.5	1.4	30	–	3.2	2.2	n
13 27 42.31	33 33 23.6	22.80	19.94	−24.2	1.6	26	–	2.2	0.0	n
13 27 51.42	33 30 53.2	17.98	15.75	−45.4	1.1	57	–	3.3	2.1	n
13 28 24.42	33 32 50.7	20.17	19.84	−36.4	2.0	25	–	1.9	0.2	n
13 28 26.50	33 30 53.4	22.34	19.91	3.7	1.9	22	–	3.0	2.8	n
13 28 27.13	33 33 09.5	20.24	18.60	31.3	2.1	44	–	4.0	1.5	n
13 28 07.66	33 30 13.8	19.88	19.46	128.8	1.6	26	–	2.3	0.4	n

Table 3. Derived parameters for stars in the UMaI sample.

α (J2000)	δ (J2000)	g	i	v_r (km s^{-1})	v_{err} (km s^{-1})	S/N (Å^{-1})	[Fe/H]	ΣCa (Å)	ΣNa (Å)	Member?
10 34 11.53	51 54 22.1	15.74	15.14	51.9	1.7	83	–	4.0	0.5	n
10 35 33.79	51 56 46.6	16.19	15.59	−9.9	1.6	58	–	4.6	0.8	n
10 34 17.26	51 57 33.6	20.16	19.25	−59.2	1.1	28	−2.4	1.1	0.1	y
10 34 22.13	51 56 10.6	20.56	19.78	−39.6	2.2	20	−1.5	2.9	0.2	y
10 34 18.21	51 56 33.8	21.43	20.75	−76.4	4.9	9	–	1.2	0.2	y
10 34 31.15	51 57 01.1	18.89	17.75	−57.2	0.7	26	−2.5	1.7	0.2	y
10 34 58.15	51 55 23.8	20.56	19.72	−59.6	5.6	9	–	1.0	0.2	y
10 35 03.55	51 56 20.1	20.91	20.12	−70.0	2.4	12	−2.2	1.1	0.2	y
10 35 17.58	51 55 33.9	19.47	18.37	−70.3	1.2	29	–	5.3	0.1	n
10 35 28.87	51 57 01.5	18.63	17.44	−57.2	0.6	25	−2.4	2.2	0.0	y
10 34 33.82	51 55 52.2	21.41	20.86	−137.5	2.5	8	–	2.2	0.3	n
10 35 31.46	51 57 11.0	18.67	17.48	49.9	1.9	41	–	3.2	0.7	n
10 35 42.86	51 56 17.7	20.06	19.16	−70.1	1.3	21	−2.0	2.1	0.1	y
10 35 23.72	51 57 16.1	21.77	20.99	−482.6	14.8	3	–	1.9	0.7	n
10 34 26.48	51 55 32.3	22.18	21.56	−69.0	4.3	6	–	1.5	0.4	y
10 34 29.72	51 54 37.6	22.03	21.42	−42.2	11.1	5	–	1.2	0.0	y
10 34 46.10	51 56 06.0	22.07	21.39	−100.8	10.8	4	–	2.9	0.5	n
10 35 09.99	51 57 30.9	21.74	21.04	−74.5	3.6	6	–	1.2	0.0	y
10 34 42.93	51 56 15.2	21.86	21.08	−58.0	2.9	6	–	1.2	0.3	y
10 34 02.55	51 54 17.6	19.24	18.49	−86.2	5.1	26	–	5.5	0.5	n
10 34 30.44	51 54 23.5	20.90	17.98	−13.4	1.9	19	–	1.3	3.3	n
10 33 59.76	51 54 39.8	21.08	19.38	−147.1	3.7	52	–	0.7	0.2	n
10 34 23.33	51 55 57.0	20.07	17.91	−8.9	1.5	25	–	2.7	1.7	n
10 34 16.12	51 57 17.5	22.64	19.83	−17.7	2.2	23	–	2.3	2.5	n
10 35 04.73	51 54 22.8	16.60	14.38	−18.1	1.1	78	–	3.8	2.3	n
10 34 37.01	51 54 39.1	20.02	19.28	−193.5	2.0	25	–	4.2	0.9	n
10 34 59.36	51 54 45.1	19.01	18.39	−43.2	1.1	28	–	1.9	0.4	n
10 35 02.33	51 55 47.8	20.56	18.44	14.3	1.5	24	–	3.1	1.7	n
10 34 53.68	51 54 54.4	20.89	19.77	−63.5	2.2	12	–	1.4	0.5	n
10 35 10.81	51 55 41.9	19.12	18.69	−75.0	1.9	30	–	2.2	0.2	n
10 34 54.62	51 54 51.7	18.57	17.90	−33.1	1.5	24	–	2.9	0.1	n
10 34 44.31	51 55 26.3	21.79	19.99	−176.8	2.5	18	–	3.9	0.8	n
10 34 40.95	51 57 09.6	22.22	19.15	−9.4	1.2	29	–	1.7	2.8	n
10 35 22.53	51 56 17.6	21.59	19.09	−36.8	1.6	27	–	2.5	2.2	n
10 34 27.92	51 58 47.1	21.55	19.22	−18.0	1.5	30	–	2.8	0.0	n
10 34 00.14	51 51 59.3	19.05	16.69	12.3	1.3	52	–	3.3	2.6	n
10 34 14.38	51 51 07.6	18.29	17.33	64.3	1.2	39	–	4.0	1.0	n
10 35 25.86	51 51 16.2	19.31	17.14	22.4	1.0	79	–	4.0	2.6	n
10 35 23.85	51 53 28.0	19.01	16.94	0.6	1.8	74	–	4.2	2.6	n
10 34 02.73	51 53 25.1	20.90	20.27	153.8	6.7	9	–	3.1	0.3	n
10 34 48.11	51 50 50.9	20.93	20.13	−56.0	1.8	12	−2.0	1.6	0.1	y
10 34 50.73	51 52 40.2	21.10	20.29	−45.5	3.1	12	−1.4	2.8	0.2	y
10 35 06.91	51 52 25.1	19.61	18.62	−42.9	2.5	36	–	4.0	1.1	n
10 35 11.49	51 51 33.1	19.77	18.92	−55.3	1.2	32	−2.3	1.5	0.3	y
10 35 42.36	51 52 16.5	20.11	19.24	12.0	2.8	24	–	3.2	0.5	n
10 35 36.70	51 53 18.4	21.18	20.46	−55.7	2.6	11	−2.0	1.3	0.2	y
10 34 08.46	51 50 48.7	22.46	21.98	−130.8	12.7	2	–	1.6	1.0	n
10 34 06.46	51 52 32.8	22.00	21.27	−405.0	5.7	5	–	1.4	0.6	n
10 34 16.41	51 55 28.6	22.33	21.71	96.9	6.3	5	–	1.4	0.0	n
10 34 38.19	51 53 39.2	21.70	21.18	−195.3	9.9	5	–	2.8	1.5	n
10 35 19.13	51 53 59.6	22.29	21.67	−63.3	7.9	4	–	26.7	0.4	y
10 34 03.70	51 50 50.8	21.04	18.72	89.5	2.1	36	–	3.3	1.8	n
10 34 09.85	51 52 01.5	20.94	18.87	−25.0	1.7	29	–	3.3	1.8	n
10 34 19.48	51 53 06.8	19.56	17.55	−20.4	1.1	40	–	4.3	2.1	n
10 34 34.92	51 51 22.7	20.62	18.66	−26.3	1.8	38	–	3.5	1.8	n
10 34 30.44	51 54 23.5	20.90	17.98	−8.3	1.7	42	–	1.6	0.0	n
10 34 11.32	51 51 49.4	21.57	18.84	55.9	2.2	40	–	1.8	3.2	n
10 34 23.10	51 52 43.0	19.03	18.68	107.3	1.9	36	–	1.9	0.7	n
10 34 37.01	51 54 39.1	20.02	19.28	−186.8	1.8	26	–	4.1	0.0	n
10 34 47.55	51 52 30.2	19.94	17.61	−28.3	1.2	51	–	3.1	2.7	n
10 35 10.01	51 51 17.9	19.54	19.12	−38.4	1.4	29	–	1.8	0.4	n
10 35 13.69	51 50 57.7	20.56	17.78	51.0	1.1	46	–	2.2	3.1	n

Table 3 – *continued*

α (J2000)	δ (J2000)	g	i	v_r (km s^{-1})	v_{err} (km s^{-1})	S/N (Å^{-1})	[Fe/H]	ΣCa (Å)	ΣNa (Å)	Member?
10 35 02.34	51 53 09.1	21.67	18.86	48.1	4.5	25	–	2.1	3.0	n
10 35 12.06	51 53 35.6	22.28	19.93	−21.5	2.7	17	–	2.8	1.7	n
10 35 16.46	51 52 15.5	21.90	19.58	−95.5	4.6	25	–	3.4	2.0	n
10 35 39.05	51 50 49.9	21.61	19.01	19.5	2.0	33	–	2.8	2.8	n
10 35 25.33	51 52 40.7	19.56	17.90	42.4	0.9	49	–	4.1	1.7	n
10 34 36.19	51 53 29.3	18.13	17.55	−19.1	1.0	57	–	3.8	1.0	n
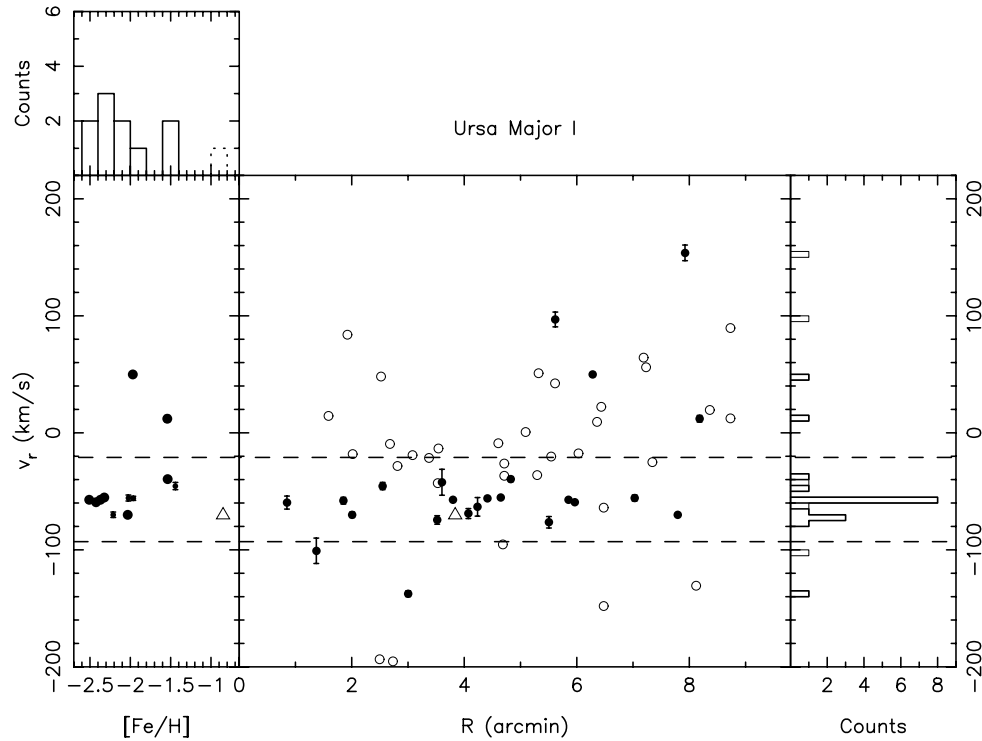
Figure 6. Same as Fig. 4 for the UMaI dwarf galaxy.

obtained by observing stars at slightly fainter magnitudes than those presented here (see Fig. 2c).

Finally, the left-hand panels of Fig. 6 confirm that UMaI is dominated by metal-poor stars with a median metallicity of [Fe/H] ∼ −2.0 although if the two most metal-rich stars that have a clear offset in metallicity and are also shifted to higher velocities than the UMaI peak are removed from the sample, this value shifts to a more metal-poor [Fe/H] ∼ −2.4. As for Boo, we have used all stars with S/N > 10 to derive the metallicity of UMaI since lower quality spectra (15 > S/N > 10, smaller filled circles in the left-hand panel) do not produce significantly different [Fe/H] values than higher quality spectra (S/N > 15, bigger filled circles).

6 URSA MAJOR II

The very faint UMaII satellite was presented in Zucker et al. (2006b) and was also discussed by Grillmair (2006). With a total magnitude of only $M_V \sim -3.8$, it would be one of the faintest known Milky Way satellites, though its structural parameters are not well constrained, with a distance of 30 ± 5 kpc and a half-light radius that could be between 50 and 120 pc. UMaII is peculiar in the sense that it lies spot on the extrapolation of the orbit of the so-called Orphan

Stream of Belokurov et al. (2006b) and Grillmair (2007), a stellar stream that extends over ∼60° on the sky at distances ranging from ∼15 kpc at its nearest extension to 30 kpc where it is nearest to UMaII (located ∼10° away). UMaII also overlaps with the detection of Complex A, an H I high-velocity cloud. The distance to the cloud, estimated between 4 and 10 kpc, however, does not favour a direct link.

One DEIMOS field was targeted at the centre of the object (see Fig. 1d where the two dashed circles represent the two boundaries of the half-light radius estimate). Although the spectra are not of lower quality than those observed for the other galaxies, the Na I doublet does not seem as efficient as for the other samples where the stars selected along the giant branch of the galaxies are clearly clumped at low values of ΣNa (Fig. 3). To avoid removing genuine UMaII stars, we relax the cut and only consider stars with ΣNa > 1.2 as foreground dwarf stars. In this way, we keep all but one star aligned along the RGB of UMaII. The radial velocity distribution of these stars is presented in Fig. 7 and shows no clear radial velocity peak (the stars parameters are listed in Table 4). The most probable UMaII members (filled circles) are distributed in two small groups of stars: one group has $v_r \sim -120$ km s^{-1}, and is composed of stars with a similar metallicity ([Fe/H] ∼ −1.8). Since it is clearly distinct
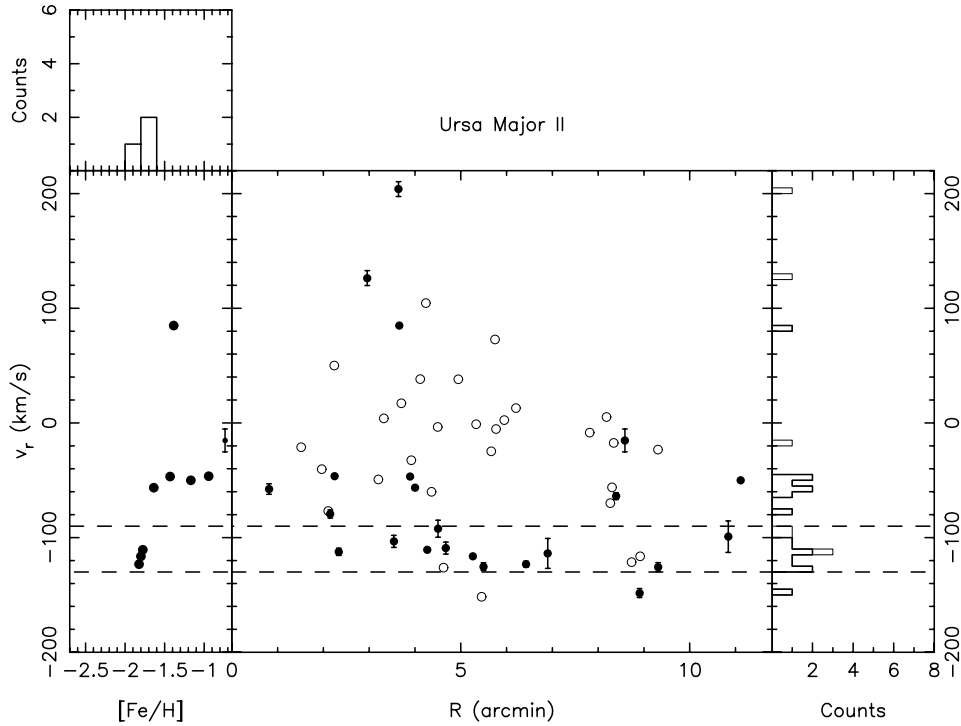
Figure 7. Same as Fig. 4 for the UMaII satellite.

from Galactic contaminants (hollow circles), and has the preferred metallicity value of Zucker et al. (2006b) for UMaII, it seems more likely that this group of stars belongs to the UMaII structure. Therefore, we henceforth only consider the group of stars with the lowest radial velocity as UMaII members ($-130 < v_r < -90 \, \mathrm{km \, s^{-1}}$; the dashed lines in Fig. 7) and assume the group with a higher velocity ($v_r \sim -50 \, \mathrm{km \, s^{-1}}$) to be made of Galactic contaminants.

UMaII is the only observed satellite that does not show a clear radial velocity peak in our survey, even though it is not the smallest of our samples. However, applying equation (1) to the probable UMaII members whatever their radial velocity uncertainty yields a dispersion of only $7.4^{+4.5}_{-2.8} \, \mathrm{km \, s^{-1}}$ around the systemic velocity $-115 \pm 5 \, \mathrm{km \, s^{-1}}$ which is not unlike what is measured in brighter dwarf galaxies such as Boo. Interestingly, these values are close to the expected value of Fellhauer et al. (2007) who have tested the hypothesis of UMaII being the progenitor of the Orphan Stream. They predict $v_r \sim -100 \, \mathrm{km \, s^{-1}}$ for UMaII and the rather high velocity dispersion we measure seem to favour their scenario of a single-component satellite of $\sim 10^5 \, \mathrm{M_\odot}$ that is on the verge of complete disruption. Unfortunately, the DEIMOS sample does not extend over a wide enough range in declination to confirm the $\sim 10 \, \mathrm{km \, s^{-1}}$ gradient they predict along this direction.

Even though UMaII seems to be the progenitor of the Orphan Stream, the radial velocity measurement rules out a direct link between UMaII and the H I velocity cloud Complex A. Indeed, according to Wakker & van Woerden (1991), the cloud has a radial velocity of $-160 \, \mathrm{km \, s^{-1}}$ whereas UMaII stars have $v_r = -115 \, \mathrm{km \, s^{-1}}$. This is not unexpected since Complex A has a distance that is lower than 10.1 kpc, much lower than that of UMaII (Zucker et al. 2006b).

7 WILLMAN 1

The peculiar object Wil1 (SDSS J1049+5103) was discovered as a very faint overdensity of stars by Willman et al. (2005a) and later

studied in more depth by Willman et al. (2006). Having characteristics between that of a globular cluster and an extremely faint dwarf galaxy, this satellite of the Milky Way has an absolute magnitude of $M_V \sim -2.5$, a half-light radius $r_{hb} = 21 \pm 7 \, \mathrm{pc}$ ($r_{hb} = 1.9 \, \mathrm{arcsec}$) and resides at a distance of $38 \pm 7 \, \mathrm{kpc}$. Deep observations reaching a magnitude $r \sim 23.5$ suggest the object may be surrounded by multiple tidal tails.

7.1 Photometry

Before analysing the DEIMOS field that was targeted on Wil1, we first present photometric data of the satellite obtained using the Wide Field Camera (WFC) mounted on the Isaac Newton Telescope (INT). One WFC pointing was observed in the V and I bands with integrations of 900 s in both bands during the night of 2004 November 20 in photometric conditions with seeing of ~ 1.0 arcsec. Reduction was performed using the version of the CASU pipeline adapted for WFC (see Irwin & Lewis 2001 for more details). To provide a comparison with a globular cluster of similar luminosity, Pal 1 was also observed during the same night and under the same conditions except for a lower exposure time (600 s for each filter). The resulting CMDs are shown in Fig. 8 with Wil1 in the left-hand panel and Pal 1 on the right-hand panel. The magnitudes of individual stars are dereddened using the Schlegel, Finkbeiner & Davis (1998) maps and transformed to SDSS magnitudes with the colour equations presented in Ibata et al. (2007). Although both objects have a similar absolute magnitude, there is a clear difference in the morphology of the main sequence of the two objects with the one of Wil1 being broader (at $g \sim 22.0$) than the main sequence of the globular cluster which harbours a single metallicity/age population ($g \sim 19$). Photometric uncertainties (reported on the right-hand side of the Wil1 panel) are too low to explain the spread of the Wil1 main sequence in colour. On the other hand, the colour difference of the Girardi et al. (2004) isochrones for an old population with

Table 4. Derived parameters for stars in the UMaII sample.

α (J2000)	δ (J2000)	g	i	v_r (km s^{-1})	v_{err} (km s^{-1})	S/N (Å^{-1})	[Fe/H]	ΣCa (Å)	ΣNa (Å)	Member?
08 50 46.29	63 04 48.6	19.46	17.39	−5.4	1.6	42	−	3.6	1.8	n
08 50 19.61	63 05 52.0	19.41	16.92	5.2	1.0	70	−	3.5	2.7	n
08 51 54.46	63 05 57.2	18.08	16.62	3.9	1.1	53	−	4.9	1.5	n
08 52 17.54	63 05 14.8	18.60	16.05	2.4	1.4	49	−	2.7	2.8	n
08 49 57.80	63 03 56.1	17.70	16.57	−50.0	1.0	76	−	4.2	1.0	n
08 50 21.25	63 04 08.7	20.68	19.96	−15.3	9.9	11	−	3.2	0.3	n
08 49 58.95	63 04 22.9	21.11	20.56	−99.2	13.7	5	−	4.0	0.3	y
08 50 58.80	63 05 54.4	18.50	17.97	−56.5	1.0	42	−	2.4	0.7	n
08 51 03.18	63 05 45.2	16.54	15.63	84.8	1.1	59	−	4.4	1.0	n
08 51 14.04	63 06 27.8	18.77	17.77	−46.5	1.3	42	−	4.0	1.1	n
08 50 12.87	63 05 58.8	21.06	20.26	−148.4	3.9	10	−	0.9	0.9	n
08 50 18.29	63 05 37.1	21.03	20.28	−63.8	2.9	9	−	3.0	0.1	n
08 50 41.90	63 06 59.6	21.50	20.86	−125.4	3.4	6	−	2.6	0.8	y
08 51 17.07	63 03 47.3	20.15	19.22	−110.6	1.7	16	−1.8	1.2	0.8	y
08 52 08.97	63 06 51.3	21.47	20.85	−92.2	7.4	6	−	2.0	0.4	y
08 51 47.21	63 04 25.8	16.59	15.68	−46.7	1.1	44	−	4.3	0.9	n
08 51 27.18	63 07 03.1	21.19	20.53	−57.7	4.6	8	−	2.7	0.0	n
08 52 09.72	63 04 41.6	21.43	20.95	−151.5	3.6	6	−	2.0	1.5	n
08 52 19.57	63 03 46.2	21.27	20.51	−113.8	13.1	8	−	1.0	0.2	y
08 51 48.45	63 06 44.7	21.59	20.95	−112.4	3.2	5	−	1.9	0.7	y
08 52 16.52	63 04 06.2	20.44	19.59	−123.2	2.5	16	−1.8	0.8	0.3	y
08 52 12.28	63 05 35.2	19.66	18.80	−116.3	1.1	26	−1.8	1.4	0.8	y
08 51 55.69	63 08 21.8	20.93	20.17	126.3	6.5	12	−	4.2	0.0	n
08 49 59.59	63 03 48.3	21.92	21.40	−587.0	13.4	3	−	1.6	2.1	n
08 50 02.28	63 05 57.6	22.33	21.60	501.8	9.5	2	−	3.3	0.5	n
08 50 08.12	63 06 46.3	21.88	21.20	−125.6	3.9	4	−	0.2	0.7	y
08 50 04.44	63 06 14.6	22.36	21.75	247.5	10.6	3	−	3.9	0.9	n
08 50 48.69	63 07 33.0	21.64	21.07	−109.2	5.2	4	−	1.2	0.0	y
08 51 16.15	63 06 19.5	21.78	21.14	−79.4	3.5	5	−	3.0	0.8	n
08 51 19.57	63 03 55.9	21.90	21.39	−286.7	14.2	3	−	2.2	0.8	n
08 51 29.23	63 04 15.7	21.73	21.12	−103.3	5.2	5	−	2.4	1.1	y
08 51 52.02	63 05 08.6	21.61	21.21	203.9	6.5	5	−	0.9	0.5	n
08 51 42.27	63 04 40.1	21.98	21.55	−396.0	6.2	3	−	0.1	1.6	n
08 50 24.93	63 03 56.9	21.49	19.22	−56.2	1.8	23	−	3.7	1.8	n
08 50 27.01	63 04 34.1	20.52	17.74	−8.5	1.0	46	−	2.1	3.3	n
08 50 54.74	63 03 46.5	18.01	15.95	−24.9	1.1	56	−	4.6	2.1	n
08 51 02.04	63 05 28.6	20.41	17.81	−32.6	0.9	44	−	3.0	2.6	n
08 50 56.08	63 06 17.9	19.42	17.64	38.2	1.3	49	−	4.5	2.1	n
08 50 20.52	63 05 13.3	17.35	15.83	−70.0	1.2	67	−	5.3	1.5	n
08 50 13.55	63 05 35.9	21.15	19.96	−116.4	7.2	9	−	4.5	0.6	n
08 50 16.55	63 06 58.3	21.60	19.36	−17.5	2.1	20	−	3.8	1.9	n
08 51 05.36	63 05 21.6	21.11	18.51	17.2	1.3	36	−	2.8	3.0	n
08 50 45.24	63 06 06.0	21.30	18.46	−1.2	1.3	34	−	2.5	3.5	n
08 50 09.75	63 05 41.8	22.58	19.73	−23.3	2.9	19	−	1.8	3.4	n
08 50 50.63	63 07 08.5	22.34	19.47	−3.6	1.8	22	−	1.8	0.0	n
08 51 44.48	63 03 45.3	19.23	17.69	−60.1	1.0	52	−	4.6	1.2	n
08 51 21.43	63 05 55.7	22.16	19.84	−76.8	8.4	12	−	3.9	1.3	n
08 52 05.07	63 03 38.0	19.83	17.55	72.7	1.0	54	−	3.8	1.4	n
08 51 49.67	63 03 44.8	20.14	20.00	−126.1	7.8	13	−	1.9	0.6	n
08 52 02.99	63 05 47.1	21.77	19.09	104.5	6.2	28	−	1.4	2.7	n
08 51 41.72	63 06 21.0	21.78	18.83	−40.3	1.8	24	−	2.1	3.2	n
08 52 15.16	63 04 16.3	21.79	19.14	12.8	1.5	25	−	2.9	2.5	n
08 51 57.96	63 08 17.5	22.21	19.84	−49.2	4.3	19	−	3.2	0.0	n
08 52 13.09	63 06 55.9	22.33	19.30	38.1	2.7	21	−	2.2	3.5	n

metallicities ranging from [Fe/H] = −2.3 to −0.7 indicates that such a metallicity spread in the satellite could explain the broadness of the main sequence observed in the satellite. This simple side by side comparison already shows that Wil1 is not a simple cluster.

We use stars within the main sequence of Wil1 to draw the radial profile of the object. The possible tidal tails of the object (Willman et al. 2006) that also appear in our data and the low number of stars prevent the construction of a detailed profile. Therefore, we simply construct the profile by determining the number of stars that are located within circular annuli at increasing distance from the centre of the object, taken as $(\alpha, \delta) = (10^h 49^m 22^s, +51°03'03''.6)$ (J2000; Willman et al. 2005a). Background correction is determined
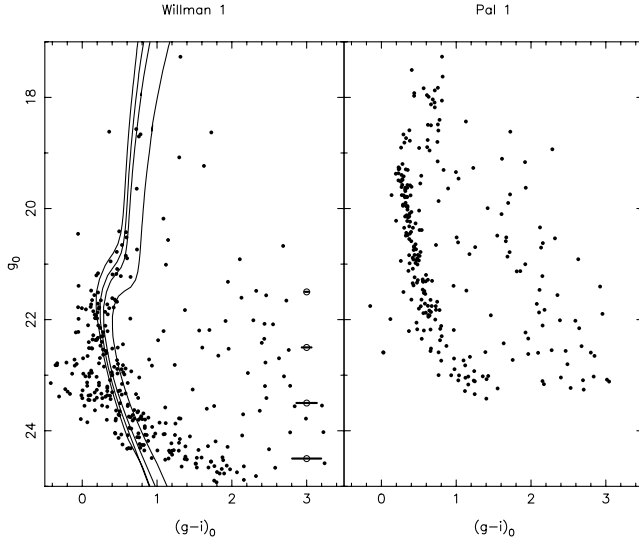
Figure 8. CMD of the region within 5 arcmin of Wil1 (left-hand panel) and the equally faint globular cluster Pal 1 (right-hand panel) in the INT/WFC data. Although in both cases the main sequence is clearly visible, that of Wil1 is broader than the single age/metallicity main sequence of Pal 1. This broadness cannot be explained by the photometric uncertainties reported on the right-hand side of the Wil1 panel. The Girardi et al. (2004) isochrones with an age of 14 Gyr and metallicities of [Fe/H] = −2.3, −1.7, −1.3 and −0.7 from red to blue have also been overlaid on the CMD. A metallicity spread covering this range could explain the broad main sequence.
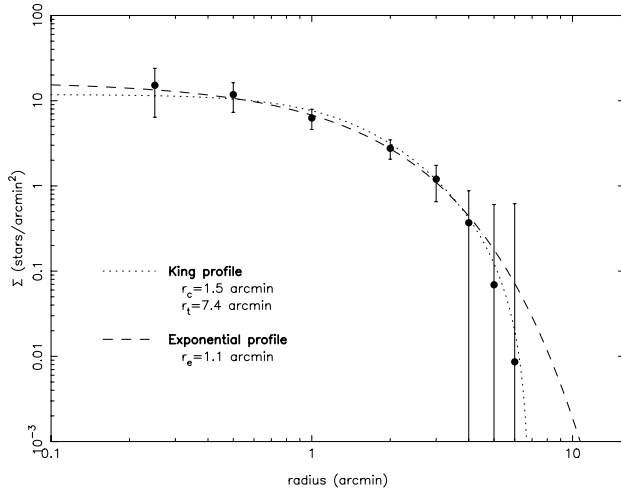
Figure 9. Radial density profile of Wil1 from the WFC data (filled circles) with error bars representing the 1σ uncertainties, including background subtraction. The dotted line represents the best King profile that can be fitted to the data within a radius of 4 arcmin while the dashed line represents the best exponential model. The respective parameters (core radius, tidal radius and exponential length) are listed in the panel.

from the number of stars within the selection box that are observed on the furthermost CCD of the detector from the one containing Wil1 ($\sim 1/3°$ away and covering 22.8×11.4 arcmin^2). The resulting profile appears in Fig. 9 with the best fits for a King model (core radius $r_c = 1.5$ arcmin and tidal radius $r_t = 7.4$ arcmin) and an exponential model (exponential length $r_e = 1.1$ arcmin). Though the fits are admittedly not perfect, the derived parameters can be used as rough estimates of the satellite structural parameters.

7.2 Spectroscopy

As before, the observed targets are shown in Fig. 1(e), the SDSS CMD of this region of the sky in Fig. 2(e) and the Na I doublet discrimination in Fig. 3(e). The usual cut at $\Sigma Na = 0.8$ Å is very useful to isolate Wil1 stars from most of the foreground contaminants. For homogeneity with the observations of the other satellites, the targets were selected from SDSS instead of the WFC observations. Given the depth reached by DEIMOS observations ($i \sim 22$), the extra depth provided by the WFC data is not needed for target selection purposes. The observed stars and their parameters are listed in Table 5.

The velocity distribution of the observed stars is shown in Fig. 10 and reveals Wil1 stars are grouped in a low-dispersion peak that is well defined even though the satellite stars (filled circles in the central panel) overlap with Galactic contaminants that have a higher dispersion (hollow circles). It is probable that some of the likely Wil1 members, selected from their location in the CMD are in fact contaminants but the low dispersion of the peak argues against a significant fraction of such objects. We, however, refrain from assigning to the Wil1 population a priori field stars with the radial velocity of the peak and that are close to this RGB as we did in the case of Boo.

As for the Boo sample, we determine the parameters of the satellite by iteratively performing a 3σ clipping and applying the same maximum likelihood technique, starting with the whole sample without the two clear outliers that appear in Fig. 10 at $v_r = 59.5$ km s^{-1} and $v_r = -74.1$ km s^{-1}. Convergence is reached for a systemic velocity of $v_r = -12.3 \pm 2.5$ km s^{-1} ($v_{gsr} = 32.4 \pm 2.5$ km s^{-1}) and a velocity dispersion of only $\sigma = 4.3^{+2.3}_{-1.3}$ km s^{-1} and higher than 2.1 km s^{-1} at the 99 per cent confidence limit which means that the observations are of a good enough quality to resolve the intrinsic dispersion of the population. Restricting the sample to the best determined objects, with $v_{err} < 6$ km s^{-1}, yields very similar values ($v_r = -13.3 \pm 2.5$ km s^{-1} and $\sigma = 4.3^{+2.6}_{-1.4}$ km s^{-1}).

Given the low velocity dispersion measured, one might get worried about the influence of binaries on the measured dispersion. The work of Olszewski, Pryor & Armandroff (1996) shows that the effect of binaries at the centre of Wil1 should be of the order of 1–2 km s^{-1}. This value should be quadratically removed from the measured dispersion reducing σ only marginally to ~ 3.8 km s^{-1}. The jitter that is known to exist in the atmosphere of red giant stars can also artificially increase the measured velocity dispersion. In the Wil1 case, however, all stars but two are more than 3 mag fainter than the tip of the RGB whereas, according to Côté et al. (1996), this is the magnitude limit at which the jitter disappears. Therefore, this should not be an issue here.

The low velocity dispersion that is measured in Wil1 is not unlike what is found in some globular clusters (e.g. Dubath, Meylan & Mayor 1997) but the results from CVnI show that (faint) dwarf galaxies can also host such low velocity dispersion populations. Moreover, globular clusters host single metallicity and age populations and the metallicity distribution of probable Wil1 members (left-hand panels of Fig. 10) shows a wide spread in metallicity. Indeed, the eight stars with S/N > 10 are scattered over $-2.0 \lesssim$ [Fe/H] $\lesssim -1.0$. Given the low dispersion of the radial velocity peak, it is also very unlikely that many of these stars are not Wil1 members. Alternatively, this large scatter could be due to our extrapolating the determination of [Fe/H] from the Ca II triplet EW down to the main-sequence turn-off or to the lower quality of the spectrum of most of these stars (15 > S/N > 10, smaller filled circles). However, there is no sign of a correlation between the metallicities

Table 5. Derived parameters for stars in the Wil1 sample.

α (J2000)	δ (J2000)	g	i	v_r (km s^{-1})	v_{err} (km s^{-1})	S/N (Å^{-1})	[Fe/H]	ΣCa (Å)	ΣNa (Å)	Member?
10 50 15.74	51 02 22.3	15.96	15.08	−51.5	1.1	88	–	5.2	0.9	n
10 48 39.51	51 04 35.7	19.85	17.41	8.7	1.3	66	–	3.5	2.5	n
10 48 46.16	51 02 12.2	19.27	17.42	55.4	1.1	65	–	3.9	1.5	n
10 49 56.99	51 05 49.5	19.36	16.66	15.7	1.2	65	–	2.2	0.0	n
10 49 12.41	51 05 44.2	18.90	18.01	−10.2	1.2	48	−0.8	4.6	0.0	y
10 49 17.43	51 03 25.9	20.55	19.90	−16.7	3.9	15	−1.7	1.4	0.1	y
10 49 16.76	51 04 03.6	21.39	20.87	−14.0	4.9	7	–	2.9	0.4	y
10 49 21.16	51 03 30.2	21.20	20.67	−22.3	14.7	8	–	1.8	0.2	y
10 49 08.09	51 02 27.0	21.04	20.32	−8.3	2.8	13	−1.1	2.5	0.1	y
10 49 15.98	51 02 26.5	21.05	20.33	−12.2	4.8	12	−1.1	2.3	0.3	y
10 48 58.13	51 02 53.9	21.36	20.75	−13.4	3.8	9	–	1.7	0.0	y
10 49 27.86	51 03 46.3	20.74	20.21	−11.7	2.8	15	−1.6	1.4	0.1	y
10 49 42.89	51 04 22.8	18.87	17.96	−13.2	1.0	49	–	4.5	1.1	n
10 49 52.54	51 03 42.5	18.75	17.89	−22.0	0.6	55	−2.1	1.6	0.4	y
10 49 40.83	51 03 40.3	21.31	20.78	−6.9	7.1	10	−1.4	1.4	0.2	y
10 49 30.96	51 03 41.0	21.34	20.81	7.3	14.1	8	–	2.3	0.1	n
10 49 10.13	51 03 00.3	21.32	21.15	−4.9	6.8	12	−1.4	1.3	0.4	y
10 49 24.36	51 02 29.3	21.49	21.38	−442.4	7.8	4	–	2.4	0.2	n
10 48 57.14	51 02 31.4	21.83	21.39	−2.4	7.9	6	–	1.5	0.1	y
10 49 23.67	51 03 03.9	22.45	21.91	−173.1	7.3	3	–	1.9	1.0	n
10 49 21.62	51 02 45.3	22.21	21.81	230.6	3.0	4	–	1.4	0.1	n
10 49 20.26	51 03 42.9	21.88	21.62	59.5	9.4	4	–	2.9	0.2	n
10 49 25.04	51 02 25.2	21.91	21.47	208.7	5.2	4	–	2.0	1.0	n
10 49 26.33	51 03 16.4	21.81	21.49	−374.9	8.4	4	–	19.4	0.3	n
10 49 31.41	51 03 02.7	21.51	21.31	498.4	7.4	9	–	0.7	0.3	n
10 49 47.37	51 03 34.7	22.00	21.87	−8.5	8.5	4	–	1.9	0.7	y
10 49 50.13	51 05 12.5	22.11	21.76	542.8	8.7	4	–	0.5	0.4	n
10 50 02.89	51 02 32.2	21.67	21.09	−7.7	4.1	8	–	3.0	0.1	y
10 49 39.00	51 04 57.4	22.14	21.85	−74.1	7.7	4	–	3.7	0.4	n
10 49 34.78	51 04 28.5	21.91	21.61	12.7	11.2	5	–	1.8	0.4	n
10 49 07.40	51 04 09.8	21.85	19.81	−2.2	2.0	22	–	3.4	1.9	n
10 49 06.85	51 04 23.6	18.77	18.33	220.4	1.1	45	–	2.5	0.4	n
10 49 03.88	51 06 40.2	17.69	15.50	−10.2	1.1	84	–	4.0	0.0	n
10 48 45.14	51 05 36.2	21.02	18.78	−39.3	2.0	34	–	3.2	2.1	n
10 48 51.58	51 03 09.9	19.77	19.32	38.6	1.4	25	–	2.2	0.3	n
10 48 48.96	51 04 15.5	22.00	19.02	−19.8	1.2	37	–	2.1	4.0	n
10 48 53.25	51 06 30.6	21.46	18.82	−24.0	1.2	38	–	2.6	0.0	n
10 48 53.65	51 06 23.8	21.67	18.82	−26.3	1.8	37	–	2.3	0.0	n
10 48 50.57	51 04 47.7	22.18	19.39	−48.9	2.3	31	–	2.1	2.9	n
10 48 58.89	51 04 56.6	22.76	19.88	10.8	2.2	21	–	1.8	3.9	n
10 49 19.54	51 04 17.3	22.28	19.71	−44.0	3.4	25	–	2.4	2.5	n
10 49 33.83	51 03 33.8	20.83	19.53	29.6	2.1	23	–	4.3	1.2	n
10 50 09.51	51 04 15.1	19.93	17.73	−94.8	2.2	46	–	3.4	1.8	n
10 49 51.71	51 05 11.8	21.99	19.70	14.6	2.4	22	–	2.8	2.2	n
10 49 54.59	51 04 16.7	22.42	19.78	28.1	1.5	25	–	2.8	2.7	n
10 50 04.57	51 03 33.0	22.93	19.98	−31.5	5.5	24	–	1.2	3.5	n
10 50 07.87	51 02 57.4	19.16	17.81	−28.5	1.1	45	–	4.8	1.5	n
10 50 01.31	51 04 43.4	21.64	18.44	14.6	1.6	38	–	1.1	4.5	n

or the metallicity spread with the magnitude of the stars whereas the isochrones overlaid on the CMD of Wil1 (Fig. 10) and ongoing statistical analysis of the SDSS CMD of this satellite reveals a similar metallicity spread (de Jong et al., in preparation). The two giant stars that have S/N > 15 are also spread over the whole metallicity range of the satellite (bigger filled circles in the bottom left-hand panel).

Hence, while the low velocity dispersion of Wil1 is not unlike that observed in globular clusters, the large metallicity spread argues strongly against such a possibility since globular clusters contain populations of a single age and metallicity. This confirms the difference that is readily visible between the main sequences of Wil1

and Pal 1 in Fig. 8. Thus we conclude that even though Wil1 is very faint and small, it is probably a dwarf galaxy. The metallicity spread could also explain the broad main sequence that is observed in Wil1 (Fig. 8).

As we have been doing for the other satellites, we estimate the mass of Wil1 from its central velocity dispersion and structural parameters assuming it is in virial equilibrium. Although this is certainly not the case given the disturbed appearance of the outskirts of the satellite as observed by Willman et al. (2006), we will nevertheless assume the following techniques provide a measure of its instantaneous mass. Equation (2) with $S_0 = 0.4 L_\odot$ pc^{-2} from the exponential profile fitted to the radial profile of Wil1 in Fig. 8 and
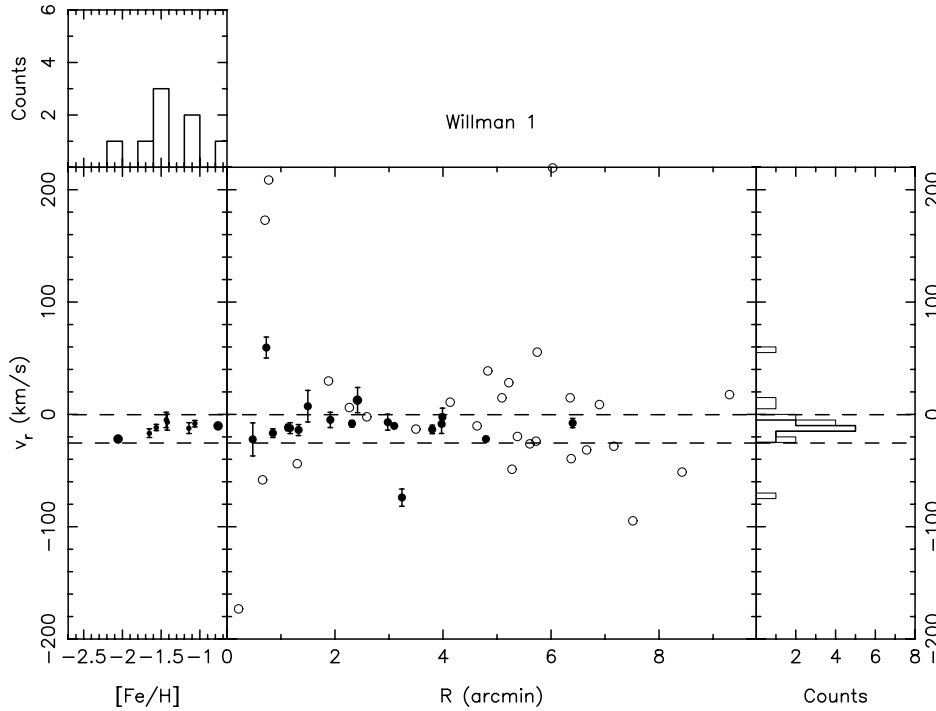
Figure 10. Same as Fig. 4 for the Wil1 dwarf galaxy.

$r_{hb} = 21$ pc leads to $(M/L) \sim 700$ in solar units (i.e. $M \sim 6 \times 10^5 \, M_\odot$). Equation (3), using the core radius measured in Section 7.1, $r_c = 16.6$ pc, yields $M = 4.0 \times 10^5 \, M_\odot$ (using r_h 5 instead of r_c as was done for the other dwarfs increases this value to $M = 5.2 \times 10^5 \, M_\odot$). With a magnitude $M_V \sim -2.5$, Wil1 has a total luminosity $L \sim 855 \, L_\odot$ which yields $(M/L) \sim 470$ in solar units. The two-mass estimates agree although neither account for uncertainties in the total luminosity of the satellite, which is as yet not well constrained. They show that Wil1 seems to be highly dark matter dominated,[4] but with a mass that is only of the order of $\sim 5 \times 10^5 \, M_\odot$.

8 DISCUSSION AND CONCLUSION

The spectroscopic observations we have performed with the DEIMOS instrument on new faint Milky Way satellites reveal that these objects are diverse and more complex than could be expected from their photometry alone (see Table 6 for a summary). In particular, UMaII does not show any clear radial velocity signal and comparison with the Fellhauer et al. (2007) simulations favours a direct link with the Orphan Stream. The other four satellites have radial velocity dispersions that are consistent with dwarf galaxies, although this does not mean they are comparable. In particular, CVnI presents a complex structure with two very distinct populations: more metal-rich stars forming a kinematically cold population at the centre of the satellite and more metal-poor stars that belong to a more extended and hotter population (Ibata et al. 2006). A similar behaviour could also be present in UMaI though our sample remains too small to derive reliable parameters for this satellite. On

the other hand, Boo and Wil1 show much cleaner radial velocity peaks.

Overall, though these objects are indeed dwarf galaxies, their median metallicity is never lower than [Fe/H] ~ -2.1 (within the metallicity scale caveat mentioned in Section 3). Therefore, the M_V–[Fe/H] relation that is found for brighter galaxies (see e.g. Mateo 1998 or fig. 9 of Martin et al. 2006) seem to break down or at least spread out at faint magnitudes. Following the previous relation, one would expect that satellites such as Boo have a metallicity of [Fe/H] ~ -2.5 and even lower for Wil1. Moreover in Boo and CVnI for which the samples are the more populated and the more reliable (since only giant or subgiant stars were targeted), there still is a dearth of very metal-poor stars, as in the brighter dwarf galaxies Sculptor, Sextans, Fornax and Carina (Helmi et al. 2006).

Similar to brighter satellites, these objects appear to be highly dark matter dominated when applying the Richstone & Tremaine (1986) or Illingworth (1976) equations – under the usual assumptions that the systems are spherical and in virial equilibrium – to estimate their M/L or mass from their central velocity dispersion. However, Wil1 appears to be a peculiar outlier to the inferred mass distribution of faint satellites. Although it does appear highly dark matter dominated with an M/L estimate ranging from ~ 470 to ~ 700, this object is at least one order of magnitude less massive ($M \sim 5 \times 10^5 \, M_\odot$) than brighter dwarf galaxies who share masses of $\sim 10^7 \, M_\odot$ or higher.

With the mass we infer, it is readily visible in Fig. 11 that Wil1 is also a clear outlier from the Mateo (1998) relation between M/L and the luminosity of a dwarf galaxies in the Local Group. This is not surprising since this relation [$M/L = 2.5 + 10^7/(L/L_\odot)$] naturally assumes that dwarf galaxies have masses higher than $10^7 \, M_\odot$. Even though the uncertainties are sizeable, Wil1 would need to be at least 10 times more massive to follow the relation. Keeping the same structural parameters, this would mean that the central velocity dispersion would have to be at least $\sqrt{10} \sim 3$ times higher than

---

[4] Using $\sigma \sim 3.8 \, \mathrm{km \, s^{-1}}$ to account for binaries reduces the mass estimates by ~ 25 per cent but does not change the conclusion that Wil1 is a dark matter dominated satellite.

Table 6. Parameters used and derived for the Milky Way satellites observed and analysed in this paper. From top to bottom are listed their heliocentric distance, half-light radius, heliocentric systemic velocity, their systemic velocity corrected from the solar motion around the Milky Way, their velocity dispersion, the *V* magnitude of the HB of the satellite that was used to derive the metallicity of their members, their median metallicity and their total mass derived through equation (3). In the case of CVnI, the parameters of the cold metal-rich and of the hot metal-poor components found by Ibata et al. (2006) are listed. For the other satellites, distances and half-light radii are taken from the references cited in the text.

	Boo	CVnI (cold component)	CVnI (hot component)	UMaI	UMaII	Wil1
D (kpc)	62 ± 3	~ 220	~ 220	~ 100	30 ± 5	38 ± 7
r_{hb} (pc)	~ 230	~ 230	~ 500	~ 250	$50 - 120$	~ 20
v_r (km s^{-1})	99.0 ± 2.1	22.5 ± 0.5	26.5 ± 1.5	-57.0 ± 3.5	-115 ± 5	-12.3 ± 2.5
v_{gsr} (km s^{-1})	106.5 ± 2.1	68.3 ± 0.5	72.3 ± 1.5	-10.6 ± 3.5	-35 ± 5	32.4 ± 2.5
σ_{v_r} (km s^{-1})	$6.5^{+2.0}_{-1.4}$	0.5 ± 0.5	$13.9^{+3.2}_{-2.5}$	$11.9^{+3.5a}_{-2.3}$	$7.4^{+4.5}_{-2.8}$	$4.3^{+2.3}_{-1.3}$
V^b_{HB}	19.5	22.4	22.4	20.5	18.1	18.6
Median [Fe/H]	-2.1	~ -1.7	~ -2.1	-2.0 to -2.4	-1.8^c	-1.5
Mass ($M_\odot$)	1.3×10^7	See Ibata et al. (2006)	See Ibata et al. (2006)	4.7×10^7	–	5×10^5

^{a}Note, however, that UMaI may contain a population with a dispersion consistent with 0 km s^{-1}; $^b V_{HB}$ has been determined from the SDSS CMDs for satellites that show such a feature (Boo, CVn, UMaI) or as $m - M + 0.7$ otherwise; ^{c}for UMaII, it has to be noted that members were selected according to their metallicity so the median metallicity given here is by selection similar to previous estimates.

the one we have measured, that is, ~ 13 km s^{-1}, which is hardly compatible with the DEIMOS observations. Does it mean that a numerous population of small satellites (such as the structurally similar Segue 1; Belokurov et al. 2006c) residing in less massive dark matter haloes than brighter dwarf galaxies ($\lesssim 10^7 \, M_\odot$) have until now eluded us? Or does it mean that Wil1 was once a more luminous and massive dwarf galaxy and that its outskirts have been stripped out by tidal interaction with the Milky Way, leaving only its central population visible at present?

First, it has to be noted that equations (2) and (3) are only valid for a system with a constant M/L. The mass estimates determined here only correspond to the central regions of the satellites where stars can be used as tracers. Therefore, it does not rule out *per se* that Wil1 could be embedded in a dark matter halo that is as massive as brighter galaxies. However, the low central mass estimate of this dark matter halo compared to the brighter galaxies would still hint at a halo with a lower central density and still make Wil1 a peculiar object.

The heating of an initially colder central population could also produce the observed velocity dispersion. While the metallicity spread that is measured within Wil1 argues against the simple disruption of a globular cluster, one could argue that Wil1 is the remnant of a CVnI-like structure with only the colder core population remaining after stripping of the hotter component by tidal interaction with the Milky Way. However, in such a scenario, a significant amount of material would have to have been stripped to explain the absence of an underlying hot component in the spectroscopic data, at odds with the photometric data that do not show tidal tails containing a significant part of the whole satellite (Willman et al. 2006). Moreover, according to Piatek & Pryor (1995) the influence of tidal interaction of the measured velocity dispersion becomes significant at high distance from the centre of the satellite whereas for the Wil1 sample that extends to $\sim 2 r_{hb}$, there is no visible increase of the dispersion with distance in Fig. 10. Although the number of stars is too low for a detailed analysis, this does not favour the presence of strong tidal tails. Thus it would seem more likely that Wil1 is a highly dark matter dominated object although it resides in a much less massive dark matter halo than those of brighter dwarf galaxies such as Boo. The small systemic velocity of this peculiar object ($v_{gsr} = 32.4$ km s^{-1}) could mean it does not have a strongly radial orbit around the Milky Way, which could in turn explain why this object has survived until now.
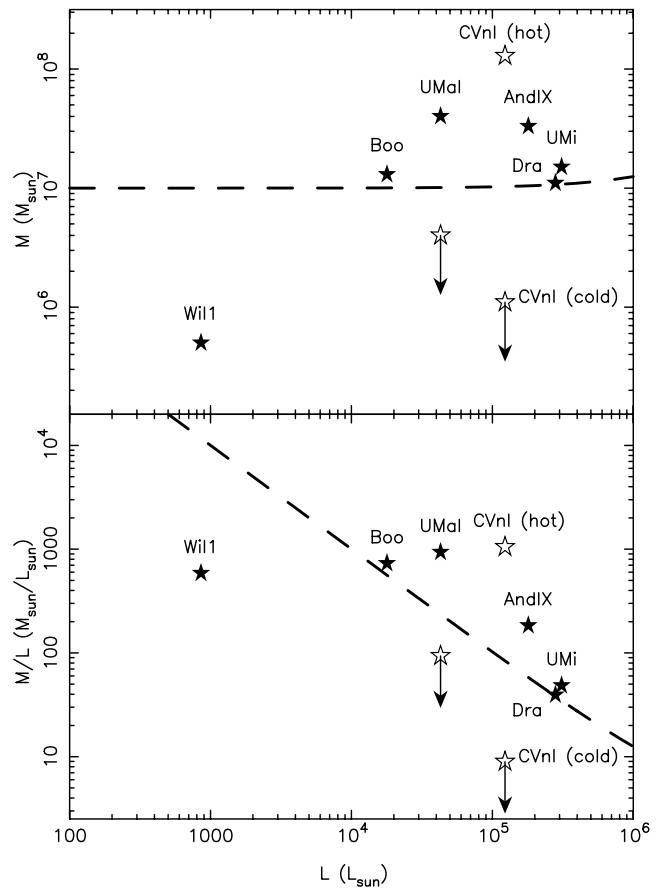

Figure 11. Comparison of the M/L values and mass estimates (M) for the faintest known dwarf galaxies with central velocity dispersion estimates (filled stars). In all cases, the mass estimates were derived using equation (3). For Draco and Ursa Minor, we use the core radii and velocity dispersions quoted in Irwin & Hatzidimitriou (1995) and Armandroff, Olszewski & Pryor (1995) respectively while we use those quoted in Chapman et al. (2005) for AndIX. For UMaI, the hollow star represent the 99 per cent confidence higher mass limit obtained from the cold component that it may harbour (see Section 5) while for CVnI, the two hollow stars represent the two diverging estimates obtained using either the cold more metal-rich half of the sample or the hot metal-poor half (Ibata et al. 2006).

Though dark matter haloes are expected to form down to planet–mass structures (Diemand, Moore & Stadel 2005), a minimum mass is required to have a deep enough potential to retain gas and eventually form stars. Therefore Wil1 could be of significant help in understanding how the lowest mass systems form if it is confirmed to inhabit a low-mass dark matter halo. Such a confirmation could come from the search for extratidal stars whose presence or absence would make it clearer if it is an unbound alignment of stars, a surviving core or a complete system. Besides, the presence of kinematically different populations in CVnI (Ibata et al. 2006) and perhaps UMaI yields significantly different mass estimates. Plotting these mass estimates in Fig. 11 (hollow stars) yields a significant spread in the mass–luminosity relation that should be taken as a warning against using *M/L* ratios when precise structural parameters are unknown. Moreover, it cannot be excluded at the moment that these satellites could have been strongly disrupted and influenced by tidal interaction or that they may have recently accreted some stellar material that did not have the time to relax in the gravitational potential of the dwarf. If this is the case, the simple application of equations (2) and (3) are not warranted and would lead to erroneous mass estimates.

The promising five new faint satellites presented by Belokurov et al. (2006b) from the analysis of the latest data release of the SDSS, with luminosities in the range $1.3 \times 10^3 \lesssim L \lesssim 2 \times 10^4 \, \text{L}_\odot$ will also undoubtedly help us understand the low-luminosity regime of dwarf galaxies between Wil1 and Boo. Spectroscopic observations for these objects are crucial to confirm if the $\sim 10^7 \, \text{M}_\odot$ limit still holds or if there is indeed a population of very faint, but not completely dark galaxies inhabiting less massive dark matter haloes that orbit within the Local Group.

ACKNOWLEDGMENTS

REFERENCES

Armandroff T. E., Olszewski E. W., Pryor C., 1995, AJ, 110, 2131
Battaglia G. et al., 2006, A&A, 459, 423
Belokurov V. et al., 2006a, ApJ, 647, L111
Belokurov V. et al., 2006b, ApJ, 654, 897
Belokurov V. et al., 2007, ApJ, 658, 337
Bullock J. S., Kravstov A. V., Weinberg D. H., 2000, ApJ, 539, 517
Carretta E., Gratton R. G., 1997, A&AS, 121, 95
Chapman S., Ibata R., Lewis G., Ferguson A. M. N., Irwin M., McConnachie A., Tanvir N., 2005, ApJ, 632, L87
Côté P., Pryor C., McClure R. D., Fletcher J. M., Hesser J. E., 1996, AJ, 122, 574
Diemand J., Moore B., Stadel J., 2005, Nat, 433, 389
Dubath P., Meylan G., Mayor M., 1997, A&A, 324, 505
Fellhauer M. et al., 2007, MNRAS, 375, 1171
Girardi L., Grebel E. K., Odenkirchen M., Choisi C., 2004, A&A, 422, 205
Grillmair C. J., 2006, ApJ, 645, L37
Harbeck D. et al., 2001, AJ, 122, 3092
Helmi A. et al., 2006, ApJ, 651, L121
Ibata R., Chapman S., Irwin M., Lewis G., Martin N., 2006, MNRAS, 373, L70
Ibata R., Martin N., Irwin M., Chapman S., Ferguson A., Lewis, G., 2007, ApJ, submitted (astro-ph/0704.1318)
Illingworth G., 1976, ApJ, 204, 73
Irwin M. J., Hatzidimitriou D., 1995, MNRAS, 277, 1354
Irwin M. J., Lewis J., 2001, New Astron. Rev., 45, 105
Kleyna J. T., Wilkinson M. I., Evans N. W., Gilmore G., 2005, ApJ, 630, L141
Klypin A., Kravstov A. V., Velenzuela O., Prada F., 1999, ApJ, 522, 82
Martin N. F., Ibata R. A., Irwin M. J., Chapman S. C., Lewis G. F., Ferguson A. M. N., Tanvir N., McConnachie A. W., 2006, MNRAS, 371, 1983
Mateo M., 1998, ARA&A, 36, 435
McConnachie A. W., Irwin M. J., 2006, MNRAS, 365, 1263
Moore B., Ghigna S., Governato F., Lake G., Quinn T., Stadel J., Tozzi P., 1999, ApJ, 524, L19
Muñoz R. R., Carlin J. L., Frinchaboy P. M., Nidever D. L., Majewski S. R., Patterson R. J., 2006, ApJ, 650, L51
Oh K. S., Lin D. N. C., Aarseth S. J., 1995, ApJ, 442, 142
Olszewski E. W., Pryor C., Armandroff T. E., 1996, AJ, 111, 750
Piatek S., Pryor C., 1995, AJ, 109, 1071
Read J. I., Pontzen A. P., Viel M., 2006, MNRAS, 371, 885
Richstone D., Tremaine S., 1986, AJ, 92, 72
Rutledge G., Hesser J., Stetson S., 1997, PASP, 109, 883
Schiavon R. P., Barbuy B., Rossi S. C. F., Milone A., 1997, ApJ, 479, 902
Schlegel D., Finkbeiner D., Davis M., 1998, ApJ, 500, 525
Siegel M. H., 2006, ApJ, 649, L83
Stoehr F., White S. D. M., Tormen G., Springel V., 2002, MNRAS, 335, L84
Tolstoy E. et al., 2004, ApJ, 617, L119
Wakker B. P., van Woerden H., 1991, A&A, 250, 509
Willman B. et al., 2005a, AJ, 129, 2692
Willman B. et al., 2005b, ApJ, 626, L85
Willman B. et al., 2006, AJ, submitted, preprint (astro-ph/0603486)
Zinn R., West M. J., 1984, ApJS, 55, 45
Zucker D. B. et al., 2004, ApJ, 612, L121
Zucker D. B. et al., 2007, ApJ, 659, 21
Zucker D. B. et al., 2006a, ApJ, 643, L103
Zucker D. B. et al., 2006b, ApJ, 650, L41

This paper has been typeset from a TeX/LaTeX file prepared by the author.